Received: 6 February 2020 | Revised: 26 May 2020 | Accepted: 31 May 2020

DOI: 10.1111/jmg.12554

ORIGINAL ARTICLE

Journal of METAMORPHIC GEOLOGY WILEY

Water in garnet of garnetite (metarodingite) and eclogite from the Erzgebirge and the Lepontine Alps

Esther Schmädicke | **Jürgen Gose**

Geozentrum Nordbayern, University Erlangen-Nürnberg, Erlangen, Germany

Correspondence
Geozentrum Nordbayern, University Erlangen-Nürnberg, Schlossgarten 5a, D-91054 Erlangen, Germany.
Email: esther.schmaedicke@fau.de

Funding information
Deutsche Forschungsgemeinschaft, Grant/Award Number: Schm1039/9-1

Abstract

Little is known about water in nominally anhydrous minerals of orogenic garnet peridotite and enclosed metabasic rocks. This study is focused on peridotite-hosted eclogite and garnetite (metarodingite) from the Erzgebirge (EG), Germany, and the Lepontine Alps (LA), Switzerland. Newly discovered, peridotite-hosted eclogite in the Erzgebirge occurs in the same ultra-high pressure (UHP) unit as gneiss-hosted coesite eclogite, from which it is petrologically indistinguishable. Garnet is present in all mafic and ultramafic high pressure (HP) rocks providing for an ideal proxy to compare the H_2O content of the different rock types. Garnet composition is very similar in EG and LA samples and depends on the rock type. Garnet from garnetite, compared to eclogite, contains more CaO (garnetite: 10.5–16.5 wt%; eclogite: 5–11 wt%) and is also characterized by an anomalous REE distribution. In contrast, the infrared (IR) spectra of garnet from both rock types reveal the same OH absorption bands that are also identical to those of previously studied peridotitic garnet from the same locations. Two groups of IR bands, SW I (3,650 ± 10 cm^{-1}) and SW II (3,570–3,630 cm^{-1}) are ascribed to structural hydroxyl (colloquially 'water'). A third, broad band is present in about half of the analysed garnet domains and related to molecular water (MW) in submicroscopic fluid inclusions. The primary content of structural H_2O, preserved in garnet domains without fluid inclusions (and MW bands), varies systematically—depending on both the location and the rock type. Garnet from EG rocks contains more water compared to LA samples, and garnet from garnetite (EG: 121–241 wt.ppm H_2O; LA: 23–46 wt.ppm) hosts more water than eclogitic garnet (EG: 84 wt.ppm; LA: 4–11 wt.ppm). Higher contents of structural water (SW) are observed in domains with molecular water, in which the SW II band (being not restricted to HP conditions) is simultaneously enhanced. This implies that fluid influx during decompression not only led to fluid inclusions but also favoured the uptake of secondary SW. The results signify that garnet from all EG and LA samples was originally H_2O-undersaturated. Combining the data from eclogite, garnetite and previously studied peridotite, H_2O and CaO are positively correlated, pointing to the same degree of H_2O-undersaturation at peak metamorphism in all rock types. This ubiquitous water-deficiency cannot be reconciled with the derivation of any of these

rocks from the lowermost part of the mantle wedge that was in contact with the subducting plate. This agrees with the previously inferred abyssal origin for part of the rocks from the LA (Cima di Gagnone). A similar origin has to be invoked for the Erzgebirge UHP unit. We suggest that all mafic and ultramafic rocks of this unit not only shared the same metamorphic evolution but also a common protolith origin, most probably on the ocean floor. This inference is supported by the presence of peridotite-hosted garnetite, representing metamorphosed rodingite.

KEYWORDS

eclogite, Erzgebirge, garnet, Lepontine Alps, metarodingite, structural water

1 | INTRODUCTION

Garnet-bearing ultramafic rocks (GBU) occurring as lenses within high-grade gneiss and granulite units represent valuable witnesses of geodynamic processes because they delineate suture zones within collisional belts (e.g. Coleman, 1971). To reconstruct orogenic processes, the setting of GBU before they were emplaced in continental crustal rocks has to be unravelled. In fact, the studied examples of GBU point to different possible sources. (a) The rocks may represent pieces from the mantle wedge that were emplaced in an underlying slab during subduction or exhumation (e.g. Brueckner, 1998; Brueckner et al., 2010; Scambelluri, Hermann, Morten, & Rampone, 2006). (b) Other examples were part of the asthenospheric mantle immediately before they came in contact with a subducting plate (Medaris, Wang, Misar, & Jelinek, 1990; Schmädicke, Gose, & Will, 2010). (c) Another possibility is that GBU originated as abyssal peridotite, in which case the ultramafic rocks were subducted together with basaltic rocks from the oceanic crust, resulting in co-facial GBU and eclogite (Evans & Trommsdorff, 1978; Evans, Trommsdorff, & Richter, 1979).

The Erzgebirge is an example of GBU associated with common, metabasaltic eclogite, but the original setting of the former is uncertain. Schmädicke and Evans (1997) interpreted the GBU as fragments from the mantle wedge that were picked up by an eclogite-bearing ultra-high pressure (UHP) slice during subduction as the UHP unit reached its maximum depth of burial. This suggestion was based on identical pressure–temperature (PT) peak conditions of GBU and coesite eclogite and the observation that GBU are absent in adjacent, less deeply subducted high-pressure (HP) units with quartz eclogite. However, this view was recently challenged, based on a comparative study of garnet-bearing peridotite and pyroxenite from the Erzgebirge and from Alpe Arami (AA), Lepontine Alps (LA; Schmädicke & Gose, 2019). The authors argued that the mantle minerals from both occurrences have the same low content of structural water (SW), which is identical to that in Erzgebirge eclogite—a finding that can much better be reconciled with an abyssal origin of peridotite. In contrast, peridotite from the base of the mantle wedge occurring directly above a subducting slab is expected to be rich in water due to the more or less continuous supply from dehydration reactions in footwall rocks.

This study was designed to further explore if the water content in nominally anhydrous minerals can be used as an indicator for the origin of orogenic GBU (i.e. ocean floor vs. mantle wedge). Compared to xenoliths, little is known about water in orogenic GBU (Peslier, 2010; Schmädicke & Gose, 2019; Yu, Wang, & Yang, 2019)—a fact that may be due to the more or less extensive retrograde overprint of orogenic peridotite and the related analytical difficulty. Nevertheless, garnet is usually well preserved, even in strongly serpentinized samples with very few olivine and pyroxene relics, and can be used as a proxy for water in the peak assemblage. In addition, garnet is present in all types of Erzgebirge GBU (peridotite, pyroxenite and garnetite; Schmädicke & Evans, 1997) as well as in eclogite (Gose & Schmädicke, 2018; Schmädicke & Gose, 2017). Therefore, it is the ideal mineral to compare the different rock types with respect to their water content. Here, we present new data on water in garnet of peridotite-hosted garnetite and eclogite from the Erzgebirge. To learn more about water in rocks hosted by orogenic GBU, garnetite and eclogite from AA and Cima di Gagnone (CG; LA) are included for comparison. Garnetite and retrogressed equivalents from the latter occurrence were interpreted as metarodingite pointing to an origin on the ocean floor (Evans & Trommsdorff, 1978; Evans et al., 1979).

2 | GEOLOGICAL SETTING

2.1 | Erzgebirge

The Erzgebirge (EG) is a rare example of UHP metamorphism linked to Variscan orogeny, with peak metamorphic ages of about 360 million years (Schmädicke, Mezger,

Cosca, & Okrusch, 1995; Schmädicke, Will, Ling, Li, & Li, 2018).The Erzgebirge consists of an 80 × 40 km large, oval-shaped, northeast-southwest trending crystalline complex that is located at the northern margin of the Bohemian Massif (Figure 1). The crystalline complex is made up of a monotonous gneiss-migmatite unit, devoid of eclogite facies relics, that is overlain by three high-pressure (HP) units (Units 1, 2 and 3), one of which (Unit 1) is an UHP unit (e.g. Klemd & Schmädicke, 1994; Schmädicke, 1994; Schmädicke et al., 1995). All three units are composed mainly of high-grade quartzofeldspatic gneiss in which meta-basaltic eclogite lenses occur as intercalations. The eclogite facies peak conditions increase systematically from Unit 3 (600–650°C, 20–22 kbar), to Unit 2 (670–730°C, 24–26 kbar) and to Unit 1 (840–920°C, ≥30 kbar; Schmädicke, 1994; Schmädicke, Okrusch, & Schmidt, 1992). Units 2 and 3 host quartz eclogite, whereas the UHP Unit 1 contains coesite eclogite (Massonne, 2001; Schmädicke, 1991, 1994) and felsic rocks with diamond (Nasdala & Massonne, 2000; Stöckhert, Duyster, Trepman, & Massonne, 2001) or diopside-albite symplectite (Schmädicke et al., 1992).

Mantle-derived, ultramafic rocks are rare in the Erzgebirge and restricted to the UHP unit. All rock types are garnet-bearing, and thermobarometric investigations provided PT peak conditions of ~900°C and 33–36 kbar that are very similar to those of coesite eclogite being part of in the same unit (Schmädicke & Evans, 1997). Garnet peridotite is the dominating rock type occurring as elongate bodies, with a length from few hundred metres up to 1–2 km, within felsic gneiss (Schmädicke & Evans, 1997). In addition, garnet pyroxenite and garnetite are also present, both of which are peridotite-hosted. The former occurs as rare, 1–15 cm thick interlayers (Mathé, 1990; Schmädicke & Evans, 1997) and the latter as boudin-like nodules of up to 30 cm in diameter, which were interpreted as metamorphosed rodingite (Schmädicke & Evans, 1997).

Erzgebirge peridotite was reported to occur in the vicinity of eclogite lenses, but both rock types were never found in direct contact (Schmädicke & Evans, 1997). However, field work and sampling in the course of this study provided evidence for peridotite-hosted eclogite nodules, though they are very rare and only occur in the quarry of Zöblitz (Figure 1). This type of peridotite-hosted eclogite is invariably associated with garnetite and also has the same shape and size as the garnetite bodies. In the course of this study, it turned out that garnetite nodules are not so rare as previously thought (Schmädicke & Evans, 1997), but occur as agglomerates in different parts of the quarry. Although garnet peridotite and pyroxenite (Schmädicke & Gose, 2019) as well as gneiss-hosted eclogite (Gose & Schmädicke, 2018; Schmädicke & Gose, 2017) were subject to recent studies on water in garnet, this investigation focuses on garnetite (metarodingite) and peridotite-hosted eclogite.

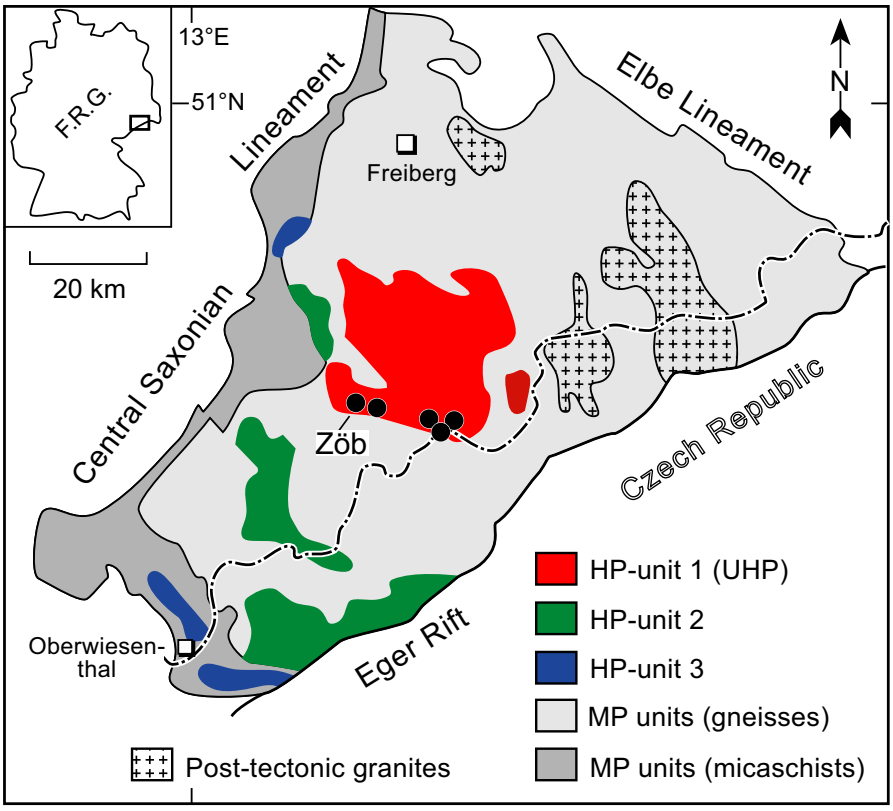

FIGURE 1 Geological map of the Erzgebirge Crystalline Complex (modified after Schmädicke et al., 1995) showing the location of the three high-*P* units, the occurrences of garnet-bearing ultramafic rocks (black dots), and the location (Zöb) of the peridotite-hosted lenses of garnetite (metarodingite) and eclogite investigated here

2.2 | Lepontine Alps

In the LA the same, rare association of peridotite-hosted garnetite and eclogite is exposed, and those rocks are included here for comparison. The former is derived from CG and the latter from AA. The rocks belong to the Adula-Cima Lunga unit, which is part of Penninic nappe pile (e.g. Schmid, Pfiffner, Froitzheim, Schönborn, & Kissling, 1996) that was subducted and metamorphosed during Alpine orogenesis (Figure 2). The metamorphic grade in the Adula-Cima Lunga unit increases from N to S providing for kyanite eclogite and associated garnet peridotite in the southern part (Evans & Trommsdorff, 1978; Heinrich, 1982, 1986). The age of HP metamorphism was confined to *c*. 37–44 Ma based on Sm–Nd dating of eclogite and garnet peridotite from AA (Becker, 1993). Eclogite from the same location gave a Lu–Hf age of 34 Ma that was attributed to partial re-equilibration following peak metamorphism at 38.8 ± 4.3 Ma (Sandmann et al., 2014). Notably, Lu-Hf dating of the eclogite from Trescolmen in the cental Adula-Cima Lunga unit testifies to a Variscan (333 Ma) and an alpine (38 Ma) metamorphic age (Herwartz, Nagel, Münker, Scherer, & Froitzheim, 2011). The authors interpreted the unit as a coherent nappe of high-*P* continental crustal rocks with intercalated mafic and ultramafic rocks.

The garnet-bearing ultramafic rocks at CG are exposed in a 200 m long lens that is in contact with both amphibolitized eclogite and gneiss (Evans et al., 1979; Pfiffner & Trommsdorff, 1998; Trommsdorff, 1990). Boudin-like bodies (few cm to 3 m in diameter) of metamorphosed rodingite and rocks transitional between eclogite and metarodingite are enclosed in the ultramafic lens. The peak conditions of eclogite (i.e., 750–800°C, 25 kbar; Brenker, Müller, & Brey, 2003) are very similar to those of garnet peridotite (800°C, >20 kbar; Evans & Trommsdorff, 1978). Both the peridotite (metamorphosed ocean-floor serpentinite) and the enclosed mafic boudins (metamorphosed tholeiite) have low-*P* precursors. The latter were interpreted as former basaltic dykes that were more or less extensively rodingitized on the ocean floor, and later on boudinaged during subduction (Evans & Trommsdorff, 1978; Evans et al., 1979; Trommsdorff, Hermann, Münterer, Pfiffner, & Risold, 2000).

The ultramafic and mafic rocks from AA, situated ~10 km apart from CG, bear no sign of previous serpentinization and rodingitization, respectively, and were interpreted as fragments from the subcontinental mantle. Reported PT peak

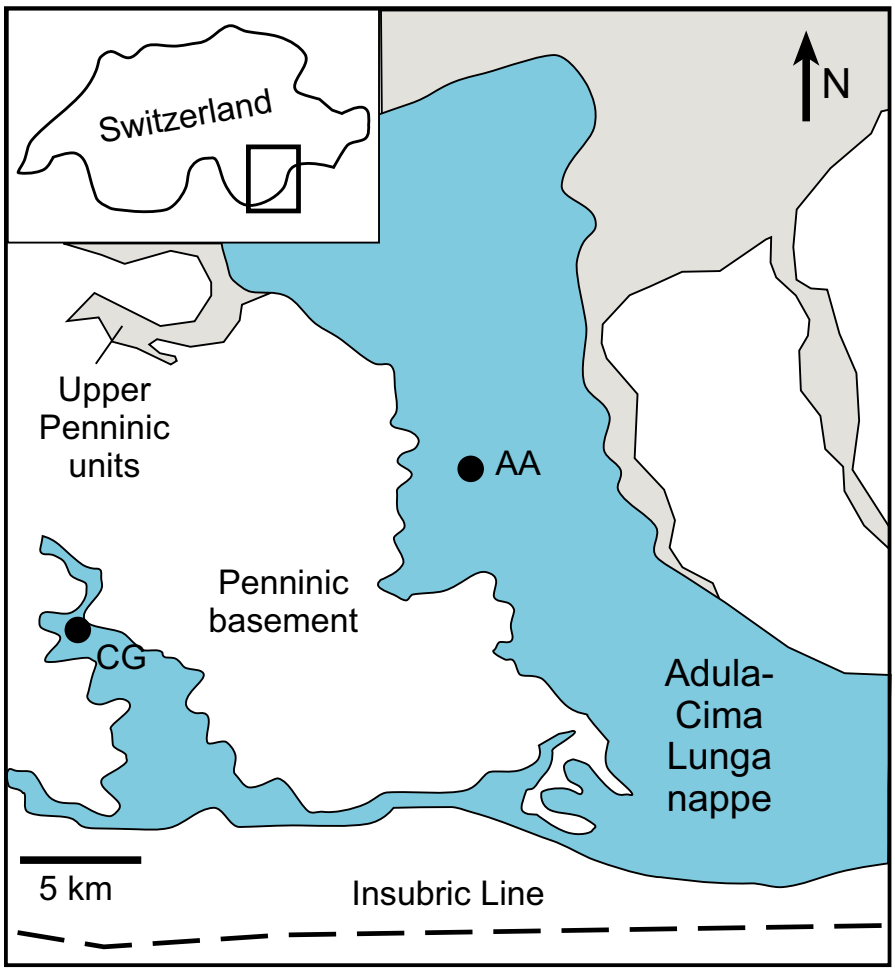

FIGURE 2 Geological map of the Adula-Cima Lunga unit (modified after Scambelluri, Pettke, Rampone, Godard, & Reusser, 2014) showing the samples locations for garnetite (metarodingite) and eclogite. AA, Alpe Arami; CG, Cima di Gagnone

conditions for AA peridotite (32 kbar and 840°C; Nimis & Trommsdorff, 2001) are very similar to those for Erzgebirge peridotite. Admittedly, there is no consensus concerning the PT peak for this locality because considerably higher PT conditions were also suggested (i.e. $P \geq 50$ kbar, $T = 1{,}100$–$1{,}200$°C; Brenker & Brey, 1997; Green, Dobrzhintskaya, & Bozhilov, 2010; Paquin & Altherr, 2001). However, the latter estimate cannot be reconciled with the results from HP experiments (Hermann, O'Neill, & Berry, 2005). At AA, meta-basaltic eclogite occurs in direct contact with a 1×0.4 km body of garnet (and chlorite) peridotite, both of which are hosted by migmatitic gneiss (O'Hara & Mercy, 1966; Möckel, 1969). The peak equilibrium temperature for AA eclogite (i.e. 800–900°C at 25 kbar; Brenker et al., 2003), again, is similar to the thermal peak in Erzgebirge coesite eclogite.

The literature data and our new observations suggest that the field appearance of peridotite-hosted garnetite (metarodingite) and eclogite in the Erzgebirge is very much alike to that of equivalent rocks from the LA. Both, the Erzgebirge high-*P* units and the Adula-Cima Lunga unit consist of HP continental crustal rocks with intercalated mafic and ultramafic rocks. In addition, a pronounced eclogite facies field gradient is common to both complexes. The same applies to the exposure of garnet peridotite and metarodingite, which, in both complexes, is restricted to the highest-grade part of the high-*P* units.

3 | SAMPLE DESCRIPTION

Thin sections were prepared and analysed from 22 samples of peridotite-hosted eclogite, garnetite (metarodingite) and retrograde equivalents (10 Erzgebirge, 4 AA and 8 CG). From the garnet-bearing samples (19), eight representative specimens (Table 1) were selected for further analysis. The following description of thin sections is focused on the peak metamorphic assemblage and the early post-peak recrystallization under late eclogitic and amphibolite facies conditions.

3.1 | Erzgebirge

The investigated Erzgebirge samples were derived from the quarry of Zöblitz (Figure 1; Table 1). A description of this outcrop was given in a previous study (Schmädicke & Evans, 1997). Peridotite-hosted *garnetite* (metarodingite) is dominated by garnet (70–75 vol.%) and diopsidic clinopyroxene (20–30 vol.%; Figure 3). Rutile and opaque minerals occur as minor phases and, in one case, biotite was observed but this sample was not selected for further analysis. Quartz is not present in any of the samples. Garnet appears in three textural types: (a) as large grains with up to 5 mm diameter, (b) as recrystallized clusters of small neoblasts (<0.2 mm grain size) that grew at the expense of some of the large grains and (c) as recrystallized grains within granoblastic garnet–clinopyroxene clusters. Clinopyroxene almost exclusively occurs in such intergrowths together with or as inclusions in garnet. Sample Zö13-3 (Table 1) investigated here is a typical example of garnetite as it occurs in several nodules in the Zöblitz quarry. In some nodules, retrogressed garnetite is present, mostly in association with non-retrogressed portions. This applies to sample Zö-Gr, in which primary garnetite and a strongly retrogressed equivalent are present in the same thin section as two separate layers (Table 1). In the retrogressed layer are garnet and clinopyroxene replaced by very fine-grained, non-identified mineral aggregates.

Peridotite-hosted *eclogite* (such as sample 113; Table 1) consists of garnet (40 vol.%) and omphacite (50 vol.%) plus minor rutile, quartz and opaque phases. Garnet has the same size (~5 mm) as the large grains in garnetite. Inhomogeneously distributed calcic amphibole occurs in interstitial positions and invariably includes vermicular or bleb-like quartz inclusions (Figure 3). This type of amphibole is a typical feature of Erzgebirge UHP eclogite as it was never found in HP eclogite. Its growth is attributed to eclogite facies recrystallization at pessures of 25–28 kbar (Gose & Schmädicke, 2018; Schmädicke et al., 1992). Post-eclogitic recrystallization is almost absent as symplectite after omphacite is present only in very small amounts («1 vol.%).

3.2 | Lepontine Alps

Garnetite (metarodingite) from CG is dominated by garnet (65–75 vol.%; Table 1). Clinopyroxene is either absent (sample CG3) or occurs in smaller amounts (sample CG5) than in Erzgebirge garnetite. Instead, calcic amphibole (both hornblende and actinolite) is a typical constituent with modal amounts of 5–15 vol.%. The textural features of sample CG5 indicate that clinopyroxene was partly consumed by hornblende. Further constituents are zoisite (<1–15 vol.%), rutile and titanite. Very fine-grained mineral aggregates occurring also in sample CG5 are not further identified. Quartz is lacking in all samples as in Erzgebirge garnetite.

The *eclogite* sample CG6-1 contains garnet and omphacite (25 and 35 vol.% respectively), a high amount of hornblende (25 vol.%) and minor zoisite, quartz and rutile. Omphacite is partially replaced by diopside-plagioclase symplectite (5 vol.%). Another type of symplectite consisting of biotite and plagioclase is inhomogeneously distributed on thin section scale and concentrated in layers (Figure 3). Such symplectites were described as rims around phengite from other eclogite occurrences and interpreted in terms of phengite decomposition (Schmädcke et al., 1992). Phengite is not observed in sample CG6-1, but the overall shape of the aggregates can well be reconciled with this

TABLE 1 Modal composition (vol.%) of peridotite-hosted eclogite and garnetite from the Erzgebirge and the Lepontine Alps and average content of main garnet end-members (mol.%)

Sample	Rock	Locality	Grs–Prp–Alm	Grt	Cpx	Cpx-Sym	Amp	Rt	Zo	Qz	Opq	Comments
Erzgebirge												
113	Eclogite	Zöblitz	30.1–26.1–42.7	40	50	+	4 hbl	2	+	3	+	hbl with qz-blebs
Zö13-3	Garnetite	Zöblitz	29.1–40.1–27.1	70	29			1		–	<1	Numerous cracks
Zö-Gr (a)	Garnetite	Zöblitz	32.8–34.5–28.1	75	20			3				aggr 2, cracks with prh?
(b)				—	—		70 act	1	+	–	<1	aggr 20, cb 6, spn 1
Lepontine Alps												
AA11	Eclogite	Alpe Arami	13.9–52.0–33.1	60	30	7		2		+	+	
AA12	Eclogite	Alpe Arami	14.7–50.5–33.7	55	35	5	+ hbl	2–3		+		hbl with qz-blebs
CG3	Garnetite	Cima di Gagnone	43.4–13.8–41.5	75			5 act	<1	15	–	1	spn 1
CG3	Garnetite	Cima di Gagnone		75			14 act	2	5	–	1	spn 3
CG5	Garnetite	Cima di Gagnone	31.4–28.0–39.0	65	7		15 hbl	5	+	–	+	aggr 7, cb?, cpx -> hbl, inhomogeneous
CG6-1	Eclogite	Cima di Gagnone	24.8–31.2–43.3	25	35	5	25 hbl	1	3	1	+	bt-pl-sym 5, inhomogeneous

Note: For abbreviations of mineral names see Whitney and Evans (2010).
aggr—very fine-grained non-identified mineral aggregates, sym—symplectite, +—trace. (a) and (b) two separate layers in same thin section.

interpretation. The mineral assemblage of AA eclogite (AA11, AA12) is very similar to that of coesite eclogite from the Erzgebirge. Apart from garnet (55–60 vol.%), omphacite (30–3 vol.%) and some symplectite after omphacite (5– vol.%), the samples contain rutile, minor quartz and hornblende. The latter reveals the same vermicular inclusions of quartz as observed in coesite eclogite from the Erzgebirge (Figure 3).

The comparison of thin sections from EG and LA samples shows that the mineral assemblages in equivalent rocks from both field areas have significant key features in common such as the presence (eclogite) or absence (garnetite) of quartz and clinopyroxene-plagioclase symplectite.

4 | ANALYTICAL DETAILS

Doubly polished, self-supporting rock slices were prepared from the same rock chips that served for thin section preparation. The thickness of the slices depends on the grain size and crystal quality of garnet and ranges between 0.2 and 0.5 mm. These specimens were utilized for all analytical tasks which were carried out in the order (a) infrared (IR) spectroscopy, (b) electron microprobe analysis and (c) laser ablation inductively coupled plasma mass spectrometry (LA-ICP-MS). Accomplishing the non-destructive IR measurements first and the most destructive analysis (ICP) last, allowed to obtain all analytical data from identical garnet grains.

The major and minor element composition of garnet was determined with a JEOL 8200 electron microprobe at conditions of 15 kV, 15 nA and a counting time of 20–40 s. The utilized instrument (University of Erlangen) is equipped with five wavelength-dispersive spectrometers. For calibration, silicate and oxide standards were used. For each sample, 10–20 spot analyses (depending on homogeneity) were collected from several garnet grains. The obtained uncertainty was ≤2% relative. Representative analyses for each sample are given in Table 2.

The trace element contents of garnet were analysed using an UP193FX laser ablation unit (New Wave Research) connected to an Agilent 7500i quadrupole ICP mass spectrometer at the University of Erlangen. Argon served as plasma and cooling gas (14.9 L/min), auxiliary gas (0. L/min) and carrier gas (1. L/min), whereas He was utilized as secondary carrier gas (0.6 L/min). The spot diameter and the repetition rate were 30–50 μm and 20 Hz respectively. The irradiance was 0.5 GW/cm^2 and the fluence 2.8 J/cm^2. Background and mineral ablation times were 20 and 25 s respectively. The garnet SiO_2 content was used for internal and the NIST SRM 612 standard for external calibration. The reference material BCR-2G (USGS) served as secondary standard to evaluate reproducibility (mostly >95%) and accuracy (mostly >92%). Data processing was carried out

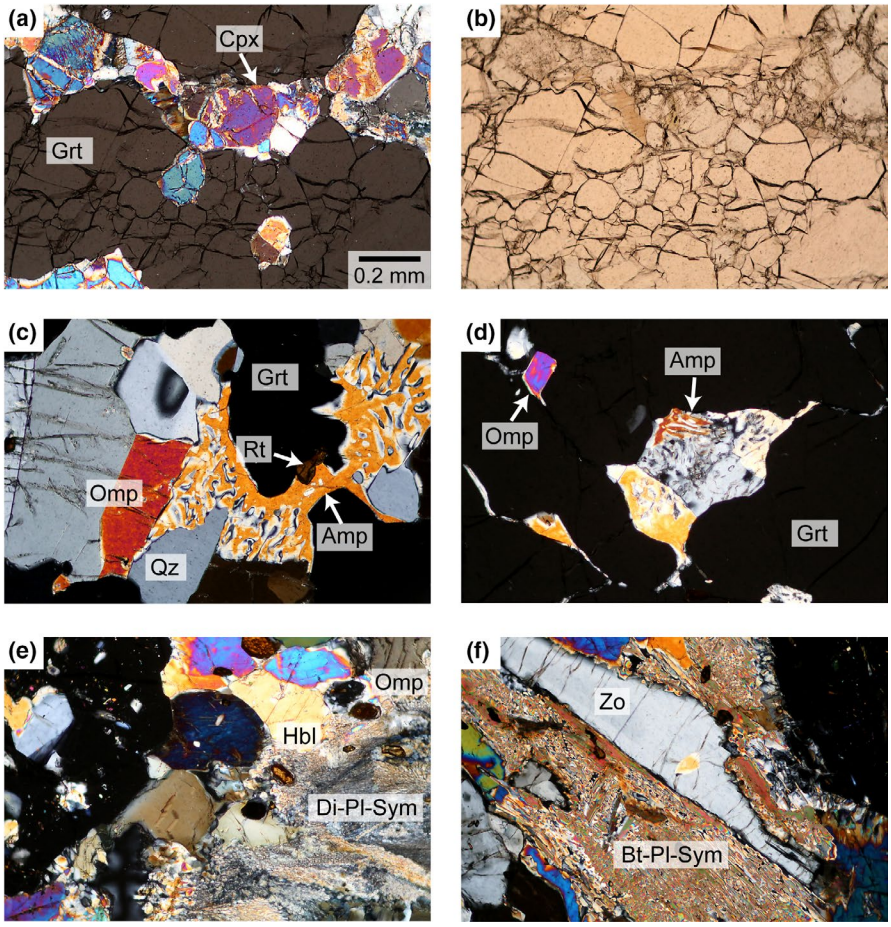

FIGURE 3 Photomicrographs of peridotite-hosted garnetite and eclogite taken with crossed polars (a, c, d, e, and f) or one polar (b) and identical magnification. (a, b) Garnetite (metarodingite) from Erzgebirge with garnet and diopsidic clinopyroxene, but no quartz. Garnet recrystallized to smaller neoblasts. (c) Erzgebirge eclogite with garnet, omphacite, quartz, rutile and post-peak calcic amphibole showing inclusions of vermicular quartz. (d) The same features, including vermicular quartz in amphibole, are present in eclogite from Alpe Arami. (e) Eclogite from Cima di Gagnone with garnet, omphacite, hornblende, rutile, and diopside-plagioclase symplectite after omphacite. (f) Eclogite from Cima di Gagnone with zoisite and biotite–plagioclase symplectite after phengite. Abbreviations are given in Table 2

with GLITTER (Van Achterbergh, Ryan, & Griffin, 2000). For each sample 4–10 (mostly 7) analyses were collected. Three typical analyses for each sample are listed in Table 3.

The H_2O concentration of garnet (given as wt.ppm or ppm respectively) was determined by Fourier transform IR spectroscopy in transmittance mode using a Vertex 70 spectrometer, equipped with a Hyperion 3000 microscope and an MCT detector at the University of Innsbruck. The IR spectra were taken with non-polarized IR radiation by averaging over 64 scans in the wavenumber range 550–7500 cm^{-1} at an instrumental resolution of 2 cm^{-1}. The spectra were collected from clear and transparent crystal volumes, free of visible inclusions, cracks and alteration products. To restrict the probed crystal volume and to exclude unsuited, impure portions, a square aperture of 30 × 30 to 100 × 100 μm^2 (in most cases ~50 × 50 μm^2) was applied. If possible, at least six spectra were collected for each crystal from different grain portions. In some cases, the available crystals were not large and clear enough so that a smaller number of different crystal volumes were analysed. The integral absorbance was calculated by fitting the spectra in the wavenumber range 3,000–3,700 cm^{-1}. The amount of water in the garnet structure (= structural water or 'SW') was inferred from the absorption of bands with maxima in the range between 3,460 and 3,670 cm^{-1} and calculated by applying the mineral-specific molar absorption coefficient of Bell, Ihinger, and Rossman (1995). For spectra fitting, deconvolution, baseline correction and quantification of H_2O, the method used for garnet from Erzgebirge eclogite (Gose & Schmädicke, 2018; Schmädicke & Gose, 2017) and GBU from Erzgebirge and LA (Schmädicke & Gose, 2019) was adopted here. The total uncertainty of the contents of SW (Table 4) is estimated to be 20% in most cases.

5 | RESULTS

5.1 | Major and trace element composition

Garnet from most samples is an intermediate solid solution of pyrope, grossular and almandine (Figure 4). Using the average analyses for each sample, the compositional range of the sample set is fairly large (Figure 4), especially if compared to recently published data for garnet from associated peridotite and pyroxenite (Schmädicke & Gose, 2019). Garnet from Erzgebirge garnetite and eclogite overlaps in composition with equivalent samples from CG, whereas eclogitic garnet from AA, being distinctly more pyrope-rich and grossular-poor, resembles peridotitic garnet (Figure 4). Garnet from garnetite of both locations generally contains more CaO (10.5–16.5 wt%) than eclogitic garnet (5–11 wt%).

TABLE 2 Selected microprobe analyses of garnet. Oxides are in wt%, cations are calculated on the basis of 12 oxygen by treating all iron as Fe^{2+}

Sample	**Zö13-3**	**Zö13-3**	**Zö-Gr**	**Zö-Gr**	**Zö-Gr**	**113**
Rock type	**Garnetite**	**Garnetite**	**Garnetite**	**Garnetite**	**Garnetite**	**Eclogite**
Grain	**grt1**	**grt2**	**grt1**	**grt1**	**grt2**	**grt1 core**
#	**3**	**8**	**29**	**30**	**37**	**127**
SiO_2	40.68	40.51	40.00	40.09	39.75	39.48
TiO_2	0.41	0.25	0.40	0.49	0.53	0.08
Al_2O_3	21.93	22.33	21.77	21.73	21.13	22.16
Cr_2O_3	0.01	0.05	0.00	0.00	0.00	0.02
NiO	0.00	0.00	0.00	0.03	0.04	0.00
FeO	13.83	13.90	14.93	14.58	15.08	21.90
MnO	0.31	0.27	0.31	0.30	0.33	0.40
ZnO	0.03	0.03	0.03	0.01	0.03	0.01
MgO	10.84	11.39	9.55	9.45	9.21	6.68
CaO	11.73	10.52	12.19	12.56	12.40	10.76
Na_2O	0.04	0.04	0.05	0.05	0.09	0.01
Total	99.80	99.29	99.22	99.29	98.60	101.51
Si	3.03	3.02	3.02	3.02	3.03	2.99
Ti	0.02	0.01	0.02	0.03	0.03	0.01
Al	1.92	1.96	1.93	1.93	1.90	1.98
Cr	0.00	0.00	0.00	0.00	0.00	0.00
Ni	0.00	0.00	0.00	0.00	0.00	0.00
Fe	0.86	0.87	0.94	0.92	0.96	1.39
Mn	0.02	0.02	0.02	0.02	0.02	0.03
Zn	0.00	0.00	0.00	0.00	0.00	0.00
Mg	1.20	1.26	1.07	1.06	1.05	0.76
Ca	0.94	0.84	0.99	1.01	1.01	0.87
Na	0.01	0.01	0.01	0.01	0.01	0.00
Total	7.99	7.99	8.00	7.99	8.00	8.02
Mg#	0.58	0.59	0.53	0.54	0.52	0.35
Uv	0.000	0.001	0.000	0.000	0.000	0.001
Sps	0.006	0.006	0.007	0.006	0.007	0.009
Grs	0.311	0.279	0.328	0.338	0.337	0.293
Prp	0.401	0.421	0.358	0.353	0.348	0.254
Alm	0.243	0.275	0.274	0.267	0.255	0.443
Sample	**AA12**	**CG3**	**CG3**	**CG3**	**CG3**	**CG5**
Rock type	**Eclogite**	**Garnetite**	**Garnetite**	**Garnetite**	**Garnetite**	**Garnetite**
Grain	**grt2**	**grt2 core**	**grt3**	**grt3**	**grt3**	**grt22**
#	29	8	14	15	20	37
SiO_2	40.58	39.36	38.55	40.27	39.07	38.99
TiO_2	0.04	0.06	0.15	0.09	0.07	0.07
Al_2O_3	23.15	21.61	21.76	22.46	21.99	21.82
Cr_2O_3	0.01	0.08	0.02	0.06	0.05	0.03
NiO	0.00	0.00	0.02	0.01	0.03	0.02

113	AA11	AA11	AA11	AA12	AA12
Eclogite	Eclogite	Eclogite	Eclogite	Eclogite	Eclogite
grt1	grt1	grt2	grt2	grt1	grt2
130	35	36	37	19	24
39.69	41.03	40.74	40.86	40.83	40.55
0.11	0.02	0.04	0.01	0.03	0.04
22.39	23.59	23.65	23.48	23.40	23.00
0.13	0.02	0.07	0.03	0.05	0.03
0.00	0.02	0.02	0.01	0.05	0.00
20.39	16.27	15.95	15.94	16.42	16.45
0.46	0.45	0.39	0.39	0.47	0.47
0.01	—	—	—	—	—
6.98	14.16	14.14	14.21	13.46	14.05
11.14	5.17	5.31	5.15	5.82	5.40
0.02	0.01	0.04	0.05	0.02	0.01
101.32	100.73	100.34	100.13	100.54	99.99
2.99	2.99	2.98	3.00	3.00	2.99
0.01	0.00	0.00	0.00	0.00	0.00
1.99	2.03	2.04	2.03	2.02	2.00
0.01	0.00	0.00	0.00	0.00	0.00
0.00	0.00	0.00	0.00	0.00	0.00
1.29	0.99	0.98	0.98	1.01	1.01
0.03	0.03	0.02	0.02	0.03	0.03
0.00	—	—	—	—	—
0.78	1.54	1.54	1.55	1.47	1.54
0.90	0.40	0.42	0.41	0.46	0.43
0.00	0.00	0.01	0.01	0.00	0.00
8.00	7.99	8.00	7.99	7.99	8.01
0.38	0.61	0.61	0.61	0.59	0.60
0.004	0.001	0.002	0.001	0.001	0.001
0.010	0.009	0.008	0.008	0.010	0.010
0.297	0.136	0.139	0.136	0.153	0.142
0.262	0.519	0.521	0.525	0.496	0.516
0.427	0.335	0.330	0.330	0.340	0.331
CG5	**CG5**	**CG6-1**	**CG6−1**	**CG6−1**	**CG6−1**
Garnetite	Garnetite	Eclogite	Eclogite	Eclogite	Eclogite
grt3	grt3	grt1 core	grt2 core	grt2 rim	rim
44	45	7	13	14	19
39.32	39.21	39.66	39.18	39.58	38.83
0.17	0.16	0.12	0.03	0.04	0.09
22.11	22.16	22.28	22.31	22.83	22.61
0.00	0.04	0.06	0.00	0.00	0.00
0.07	0.00	0.00	0.02	0.01	0.01

(Continue)

TABLE 2 Continued

Sample	AA12	CG3	CG3	CG3	CG3	CG5
Rock type	Eclogite	Garnetite	Garnetite	Garnetite	Garnetite	Garnetite
Grain	grt2	grt2 core	grt3	grt3	grt3	grt22
FeO	16.36	17.79	22.76	12.80	18.65	18.65
MnO	0.46	1.11	0.30	0.22	0.16	0.79
ZnO	–	–	–	–	–	–
MgO	13.98	4.68	1.40	8.65	3.84	6.77
CaO	5.22	15.88	15.64	15.52	16.43	11.94
Na_2O	0.03	0.00	0.00	0.01	0.03	0.00
Total	99.83	100.57	100.59	100.09	100.30	99.08
Si	2.99	3.01	3.01	3.00	3.00	3.00
Ti	0.00	0.00	0.01	0.01	0.00	0.00
Al	2.01	1.95	2.00	1.97	1.99	1.98
Cr	0.00	0.01	0.00	0.00	0.00	0.00
Ni	0.00	0.00	0.00	0.00	0.00	0.00
Fe	1.01	1.14	1.48	0.80	1.20	1.20
Mn	0.03	0.07	0.02	0.01	0.01	0.05
Zn	–	–	—	—	—	—
Mg	1.54	0.53	0.16	0.96	0.44	0.78
Ca	0.41	1.30	1.31	1.24	1.35	0.99
Na	0.01	0.00	0.00	0.00	0.00	0.00
Total	8.00	8.01	7.99	8.00	8.00	8.00
Mg#	0.60	0.32	0.10	0.55	0.27	0.39
Uv	0.000	0.002	0.000	0.002	0.002	0.001
Sps	0.010	0.025	0.007	0.005	0.003	0.017
Grs	0.138	0.442	0.439	0.417	0.451	0.331
Prp	0.514	0.182	0.055	0.324	0.147	0.261
Alm	0.338	0.349	0.499	0.253	0.398	0.390

Note: Mg#=Mg/(Mg+Fe); –, not determined.

Garnet in Erzgebirge garnetite has a composition of 31–43 mol.% pyrope, 24–36 mol.% grossular and 24–34 mol.% almandine, with Mg# of 0.51–0.59. Different grains in the same sample have somewhat variable composition but zoning does not occur. The large grains have somewhat higher CaO contents (~0.5 wt% difference) than the smaller neoblasts. Compared to garnetite, garnet from eclogite sample 113 has a similar grossular content (29–31 mol.%), but significantly lower Mg# (0.35–0.38) and pyrope (25–27 mol.%) as well as higher almandine contents (41–44 mol.%).

Garnet from the CG samples is strongly heterogeneous (pyrope: 5–37 mol.%, grossular: 17–45 mol.%, and almandine (25–50 mol.%) with Mg# ranging from 0.10 to 0.55. However, excluding sample CG3, the compositional range is much smaller (i.e. pyrope: 26–37 mol.%, grossular: 17–33 mol.%, almandine: 38–50 mol.%, Mg#: 0.39–0.44). Garnet from AA eclogite is fairly homogeneous (Mg#: 0.59–0.61, pyrope: 49–52 mol.%, grossular: 13–15 mol.%, almandine: 33–34 mol.%).

The Cr_2O_3 content is very low in all analysed grains (≤0.1 wt%), and eclogitic garnet from both Erzgebirge and AA is also poor in TiO_2 (≤0.1 wt%). Garnet of garnetite from both CG (up to 0.25 wt%) and Erzgebirge (up to 0.57 wt%) contains distinctly more TiO_2. Other, relatively abundant trace elements are Na (41–486 ppm), P (19–253 ppm), V (37–451 ppm) and Y (10–240 ppm). The Na contents of garnet from the EG samples (162–486 ppm) are significantly higher compared to LA samples (41–198 ppm). In addition, garnet in Erzgebirge eclogite has significantly lower Na concentrations (162–235 ppm) compared to that of garnetite (194–486 ppm); in contrast, no difference in Na content is observed for eclogitic and rodingitic garnet from the LA. Erzgebirge garnet also tends to have more P and V as well as less Y than Alpine garnet, albeit the concentrations overlap to

CG5	CG5	CG6-1	CG6−1	CG6−1	CG6−1
Garnetite	Garnetite	Eclogite	Eclogite	Eclogite	Eclogite
grt3	grt3	grt1 core	grt2 core	grt2 rim	rim
18.49	18.05	19.93	23.44	21.26	21.70
0.71	0.67	0.23	0.60	0.42	0.16
–	–	–	–	–	–
8.02	7.32	7.94	8.28	9.94	6.91
10.73	11.84	10.23	6.46	6.42	10.04
0.03	0.03	0.03	0.00	0.03	0.06
99.64	99.47	100.46	100.31	100.52	100.42
2.99	2.99	3.00	2.99	2.98	2.96
0.01	0.01	0.01	0.00	0.00	0.01
1.98	1.99	1.99	2.01	2.03	2.04
0.00	0.00	0.00	0.00	0.00	0.00
0.00	0.00	0.00	0.00	0.00	0.00
1.18	1.15	1.26	1.50	1.34	1.39
0.05	0.04	0.02	0.04	0.03	0.01
—	—	—	—	—	—
0.91	0.83	0.90	0.94	1.12	0.79
0.88	0.97	0.83	0.53	0.52	0.82
0.00	0.00	0.00	0.00	0.00	0.01
8.01	8.00	8.00	8.00	8.01	8.02
0.44	0.42	0.42	0.39	0.45	0.36
0.000	0.001	0.002	0.000	0.000	0.000
0.015	0.014	0.005	0.013	0.009	0.004
0.294	0.322	0.276	0.177	0.174	0.277
0.306	0.278	0.300	0.315	0.374	0.265
0.385	0.384	0.417	0.496	0.443	0.454

some extent and the difference is less pronounced compared to Na.

If the average composition of garnet for each sample is used, together with published data for garnet from associated peridotite and pyroxenite, a negative correlation is observed for both CaO-MgO ($r = -.95$; Figure 5a) and CaO-FeO ($r = -.94$; not shown) and a positive one for Na_2O-TiO_2 ($r = .89$; Figure 5b). Considering all individual analyses, positive correlations are observed for the element pairs P-Zr (Figure 5c), Hf-Zr (Figure 5d) and Na-Zr (Figure 5e). Consequently, Na is also positively correlated with Hf (not shown). The majority of analyses also reveal a positive correlation between Na and light (L) REE (e.g. Nd; Figure 5f) as well as heavy (H) REE (not shown).

The normalized REE patterns of eclogitic garnet are very similar in three investigated samples, including EG and LA occurrences (Figure 6a). The LREE are strongly fractionated resulting in a steep positive slope from La to Sm, whereas fractionation of HREE is comparably weak or absent. The overall HREE/LREE fractionation is somewhat stronger in garnet from AA eclogite compared to the Erzgebirge eclogite. In contrast, garnet from the fourth eclogite sample (CG6-1) has a 'negative hump' in the range of the medium (M) REE, causing a sinusoidal-like normalized pattern (garnet average; Figure 6a).

The REE patterns of garnet from garnetite are more variable compared to eclogite and differ from sample to sample (Figure 6b). Only garnet from sample CG3 has a REE pattern similar to that of eclogite. The curves of the EG samples Zö13-3 and Zö-Gr show strongly increasing normalized concentrations from La to Nd, moderately increasing ones from Nd to Sm and decreasing contents from Sm to Lu, causing a MREE hump. The curve of sample CG5 shows a steep-positive slope from Ce to Eu and a flat, slighly decreasing trend

TABLE 3 Selected LA-ICP-MS analyses of garnet. Concentrations are given in wt.ppm

Sample	113	113	113	Zö13–3	Zö13–3	Zö13–3
Rock type	Eclogite	Eclogite	Eclogite	Garnetite	Garnetite	Garnetite
#	grt5-3	grt6-1	grt6-3	grt2-2	grt2-3	grt3-3
Li	<0.1	0.16	0.20	0.33	0.40	0.21
B	1.2	0.80	1.1	1.2	1.1	1.4
Na	216	191	235	294	259	317
P	43	57	139	217	206	215
Sc	66	84	69	67	59	56
Ti	—	—	—	—	—	—
V	94	146	174	346	343	350
Cr	—	—	—	—	—	—
Co	53	47	48	57	57	57
Ni	—	—	—	—	—	—
Zn	—	—	—	—	—	—
Ga	3.7	8.1	13	17	17	17
Ge	4.6	3.3	2.8	1.7	1.9	1.7
Sr	0.33	0.64	0.72	0.63	0.69	0.88
Y	27	76	70	11	13	14
Zr	4.2	7.1	7.6	21	20	23
Nb	<0.006	<0.007	<0.01	<0.006	<0.01	<0.005
Ba	0.050	<0.03	0.044	<0.04	<0.05	<0.02
La	0.012	0.010	<0.009	0.046	0.029	0.031
Ce	0.29	0.19	0.26	0.48	0.51	0.54
Pr	0.18	0.15	0.17	0.25	0.25	0.29
Nd	2.2	2.7	3.0	3.6	3.7	4.3
Sm	2.0	3.4	3.7	3.9	3.6	4.3
Eu	0.84	1.6	1.6	1.1	1.1	1.2
Gd	2.5	7.5	7.4	4.1	3.8	4.0
Tb	0.45	1.5	1.5	0.48	0.50	0.52
Dy	3.2	12	12	2.6	2.9	3.2
Ho	0.77	2.7	2.6	0.42	0.50	0.54
Er	3.8	8.5	7.3	0.92	1.4	1.3
Tm	0.96	1.3	1.0	0.15	0.18	0.17
Yb	12	9.1	7.0	1.1	1.2	1.1
Lu	2.4	1.4	0.89	0.15	0.14	0.14
Hf	0.032	0.095	0.12	0.43	0.35	0.44
Ta	<0.004	<0.004	<0.005	<0.002	<0.004	<0.005
Pb	0.81	0.66	0.55	0.47	0.60	0.29
Th	<0.005	<0.005	<0.01	0.092	0.045	0.065
U	0.017	0.010	0.023	0.13	0.11	0.13

Sample	AA12	AA12	AA12	CG3	CG3	CG3
Rock type	Eclogite	Eclogite	Eclogite	Garnetite	Garnetite	Garnetite
#	2	3	5	2	5	8
Li	0.53	0.98	0.72	0.32	2.0	0.78

Zö-Gr	Zö-Gr	Zö-Gr	AA11	AA11	AA11
Garnetite	Garnetite	Garnetite	Eclogite	Eclogite	Eclogite
grt1-2	grt1-3	grt2-3	3	6	8
0.52	1.1	1.0	<0.2	<0.2	0.26
1.2	1.4	0.99	390	229	309
419	476	486	168	87	184
253	179	191	188	94	212
78	76	67	35	39	34
—	—	—	247	122	228
438	362	451	66	37	49
—	—	—	333	91	312
50	48	51	86	76	82
—	—	—	17	11	16
—	—	—	88	80	86
19	17	19	8.3	6.4	7.6
1.8	2.0	2.1	3.5	2.6	2.8
1.1	1.3	1.1	0.10	0.091	0.095
26	23	21	99	90	99
27	28	23	7.6	3.0	6.0
<0.003	<0.004	<0.009	<0.01	<0.01	<0.02
<0.03	<0.04	<0.04	<0.06	<0.06	<0.08
0.077	0.063	0.065	<0.008	<0.01	<0.008
0.73	0.87	0.94	0.034	0.022	0.040
0.41	0.52	0.47	0.034	0.035	0.055
6.2	7.6	6.7	0.84	0.84	0.96
5.6	5.9	5.1	3.3	2.4	2.3
1.5	1.4	1.3	1.5	1.2	1.4
5.4	4.4	4.1	11	7.7	8.8
0.77	0.65	0.55	2.5	1.9	2.2
5.0	4.6	3.8	20	16	18
1.00	0.87	0.84	3.9	3.4	4.2
2.8	2.4	2.3	10	11	13
0.37	0.31	0.31	1.5	1.6	2.0
2.6	2.2	2.1	10	12	16
0.35	0.29	0.34	1.2	1.6	2.2
0.58	0.66	0.49	0.18	0.031	0.11
<0.004	<0.003	<0.003	<0.007	0.0040	0.0031
0.50	0.56	0.64	<0.02	0.075	0.073
0.12	0.15	0.12	0.00098	<0.008	<0.005
0.17	0.23	0.27	0.016	0.012	0.0060
CG5	**CG5**	**CG5**	**CG6−1**	**CG6−1**	**CG6−1**
Garnetite	Garnetite	Garnetite	Eclogite	Eclogite	Eclogite
2	3	5	4	5	8
0.39	0.66	0.61	0.94	0.86	1.9

Sample	AA12	AA12	AA12	CG3	CG3	CG3
Rock type	Eclogite	Eclogite	Eclogite	Garnetite	Garnetite	Garnetite
#	2	3	5	2	5	8
B	2.8	3.2	2.4	3.5	1.5	2.5
Na	132	95	149	42	79	89
P	128	106	176	38	20	28
Sc	38	38	38	37	21	19
Ti	183	164	190	345	656	783
V	55	55	60	181	166	146
Cr	358	273	305	224	48	17
Co	66	65	66	51	25	23
Ni	12	10	15	3.1	1.2	1.5
Zn	81	76	77	57	23	23
Ga	8.4	6.6	6.5	12	8.5	10
Ge	1.6	2.3	2.5	3.9	5.7	4.2
Sr	0.086	0.11	0.077	0.13	0.13	0.053
Y	91	90	95	41	27	22
Zr	2.9	3.3	4.9	6.3	2.4	2.0
Nb	<0.02	<0.03	<0.02	<0.02	0.017	0.013
Ba	<0.3	<0.1	0.018	<0.06	0.11	<0.06
La	<0.02	<0.02	<0.02	0.0045	<0.01	<0.007
Ce	0.047	0.041	0.054	<0.009	<0.006	<0.009
Pr	0.043	0.057	0.052	0.015	<0.008	0.0034
Nd	0.86	0.92	1.0	0.29	<0.05	<0.03
Sm	2.7	2.4	2.4	2.7	<0.08	0.053
Eu	1.3	1.2	1.1	2.8	0.089	0.094
Gd	8.1	8.1	7.3	11	0.51	0.84
Tb	1.9	1.8	1.7	1.9	0.26	0.36
Dy	15	15	16	10	3.1	3.6
Ho	3.2	3.4	3.5	1.8	0.99	0.89
Er	9.0	9.7	10	4.6	3.5	2.6
Tm	1.4	1.5	1.5	0.67	0.58	0.37
Yb	9.1	10.0	11	5.1	4.1	2.8
Lu	1.2	1.4	1.6	0.75	0.69	0.45
Hf	<0.03	<0.05	0.11	0.092	<0.03	0.044
Ta	<0.01	<0.01	<0.02	0.0013	<0.009	<0.007
Pb	0.037	0.071	<0.04	0.079	0.33	0.14
Th	0.0042	<0.00	<0.02	<0.007	<0.006	0.0068
U	<0.01	0.016	0.016	0.0010	<0.007	<0.01

Note: –, not determined.

from Eu to Lu. The individual analyses of various garnet grains from the same sample commonly yield fairly uniform REE patterns. However, this does not apply to sample CG6-1 that is characterized by highly variable REE concentrations in different garnet grains (Figure 6c).

5.2 | IR spectra and band assignment

Garnet from all samples reveals IR absorption bands due to SW, although, in some cases, the bands may be very small. Despite of different band intensities, the type of IR

CG5	CG5	CG5	CG6−1	CG6−1	CG6−1
Garnetite	Garnetite	Garnetite	Eclogite	Eclogite	Eclogite
2	3	5	4	5	8
<0.7	<0.7	<0.7	2.3	3.8	2.6
88	116	83	157	108	191
31	45	36	37	57	52
25	25	27	117	67	100
467	490	446	199	159	487
136	138	135	59	50	93
106	114	149	241	201	92
48	49	47	57	62	53
4.7	7.4	3.9	3.6	4.7	1.8
25	27	22	64	65	57
5.8	6.1	5.2	3.9	4.4	7.7
3.7	3.6	4.3	3.1	2.9	4.3
0.043	0.034	0.052	0.025	0.027	8.2
58	58	76	58	39	240
3.8	4.8	3.3	13	1.8	2.6
<0.01	<0.01	<0.02	<0.02	0.0026	<0.03
<0.08	<0.06	0.070	<0.06	<0.09	4.0
<0.008	0.011	<0.02	<0.02	<0.009	1.0
<0.01	0.0072	<0.01	0.0045	0.0017	3.2
<0.01	0.012	0.014	<0.01	0.012	0.32
0.37	0.38	0.26	0.024	<0.07	2.5
2.1	1.9	1.8	<0.05	0.086	0.73
2.2	2.0	2.4	0.062	0.13	0.43
5.5	5.9	8.1	0.47	0.73	2.5
1.1	1.4	1.6	0.33	0.33	1.9
9.8	11	13	5.8	4.9	31
2.1	2.1	2.8	2.4	1.6	10
5.5	5.8	7.3	11	6.0	35
0.74	0.92	1.0	2.4	0.98	5.9
5.1	6.4	6.9	20	7.9	38
0.67	0.94	1.1	3.7	1.4	4.5
0.093	0.057	0.057	0.28	<0.02	0.13
<0.01	<0.01	0.0085	<0.01	0.0052	<0.02
0.035	<0.03	0.63	0.064	<0.04	0.090
<0.007	<0.007	<0.008	0.0078	<0.01	0.027
<0.005	<0.01	<0.01	0.0034	<0.010	0.012

absorption pattern of garnet is very similar for samples from both the Erzgebirge and the LA. Typical IR absorption bands that are attributed to SW appear at 3,570 ± 10 cm^{-1}, at 3,650 ± 10 cm^{-1}, and in the wavenumber range 3,600–3630 cm^{-1} (Figure 7). In analogy to peridotitic and pyroxenitic garnet from the same localities as the present samples (Schmädicke & Gose, 2019), the IR bands centred at 3,650 ± 10 cm^{-1} are designated as 'SW type I' and those in the 3570–3630 cm^{-1} range as 'SW type II'.

TABLE 4 Content of structural (SW) and molecular water (MW) in garnet (given in wt.ppm H_2O) of peridotite-hosted eclogite, garnetite and meta-rodingite from Erzgebirge (EG), Alpe Arami (AA) and Cima Di Gagnone (CG). The primary content of structural water is preserved in domains with very little or no molecular water (i.e. domains with ≤20 ppm MW). See text for further explanation

Sample (#)	Domains with ≤500 ppm MW				Domains with ≤100 ppm MW				Domains with ≤20 ppm MW			
	SW I	SW II	SW total	MW	SW I	SW II	SW total	MW	SW I	SW II	SW total	MW
Rock type	Average range	Average range	Average range	Average range	Average range	Average range	Average range	Average range	Average range	Average range	Average range	Average range
113	20	142	162	126	9	74	84	6	9	74	84	6
Eclogite EG	5–60	40–380	49–426	0–455	5–14	40–102	49–113	0–17	5–14	40–102	49–113	0–17
Zö13-3	10	114	124	2	10	114	124	2	11	111	121	0
Garnetite EG	0–34	71–189	76–222	0–37	0–34	71–189	76–222	0–37	1–34	71–190	76–222	0–0
Zö-Gr	10	248	258	51	10	231	241	18	12	230	241	0
Garnetite EG	0–35	126–496	129–496	0–433	0–35	126–312	129–328	0–84	0–29	126–312	129–328	0–0
AA11	0	68	68	138	0	1	2	25	1	3	4	14
Eclogite	0–1	0–195	0–195	14–351	0–1	0–3	0–4	14–31	—	—	—	—
AA12	2	6	8	2	2	6	8	2	2	6	8	2
Eclogite	1–3	3–11	6–13	0–6	1–3	3–11	6–13	0–6	1–3	3–11	6–13	0–6
CG3	7	35	42	10	7	35	42	10	8	38	46	0
Garnetite	0–11	15–45	15–55	0–58	0–11	15–45	15–55	0–58	4–11	27–45	32–55	0–1
CG5	3	20	23	1	3	20	23	1	3	20	23	1
Garnetite	2–3	13–27	15–30	0–4	2–3	13–27	15–30	0–4	2–3	13–27	15–30	0–4
CG6-1	4	7	11	3	4	7	11	3	4	7	11	3
Garnetite	3–5	0–26	5–30	0–18	3–5	0–26	5–30	0–18	3–5	0–26	5–30	0–18

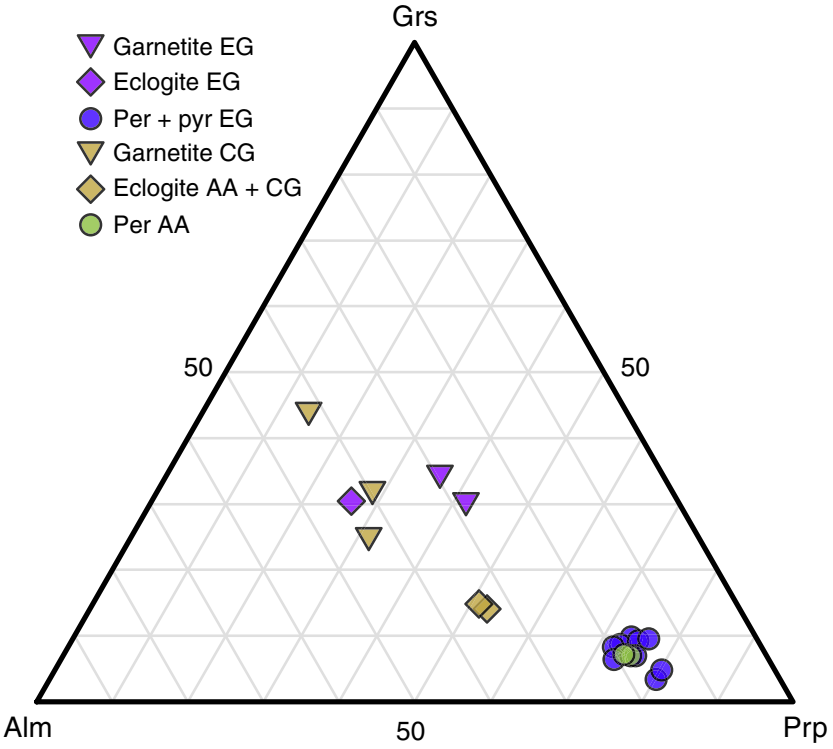

FIGURE 4 Triangle plot showing the average composition of garnet in each sample in terms of the main end members pyrope, grossular and almandine. The analyses of garnet peridotite and pyroxenite are from Schmädicke and Gose (2019). AA, Alpe Arami; CG, Cima di Gagnone; EG, Erzgebirge; per, peridotite; pyr, pyroxenite

Further bands centred at wavenumbers <3,460 cm^{-1} occur in about half of the probed garnet domains, especially in samples from the Erzgebirge (Figure 7). Such bands are ascribed to molecular water and designated as 'MW' or 'type M' bands respectively. This assignment is supported by the half width of the MW bands, being two to three times greater compared to SW bands. In addition, the intensity of MW bands is highly irregular on grain scale, which can best be reconciled with inhomogeneously distributed inclusions with liquid water. Especially some of the Erzgebirge samples reveal bands at wavenumbers ≥3,680 cm^{-1} that are highly variable in intensity and indicative of secondary amphibole (Skogby, Bell, & Rossman, 1990).

All observed bands were also described for garnet from Erzgebirge and AA peridotite and pyroxenite (Schmädicke & Gose, 2019). The SW I band is a typical feature of mantle garnet and present in peridotite, pyroxenite and mantle eclogite (e.g. Schmädicke, Gose, Reinhardt, Will, & Stalder, 2015; and references therein), but it was also found in less pyropic garnet of crustal eclogite (Gose & Schmädicke, 2018; Schmädicke & Gose, 2017). The same band was also generated by HP experiments in natural, impure pyrope (e.g. Lu & Keppler, 1997), but not in end-member pyrope (Withers, Wood, & Carroll, 1998). Up to now, the specific OH substitution mechanism for bands around 3,650 cm^{-1} is subject to discussion.

Bands in the range 3570–3630 cm^{-1} are attributed to different substitutions. Those centred between 3,585 and 3,630 cm^{--1} are ascribed to the hydrogarnet substitution, that is tetrahedral $(OH)_4^{4-}$ replacing SiO_4^{4-} tetrahedra. Such bands were reported for a variety of garnet types including synthetic end-member pyrope (Geiger, Langer, Bell, Rossman, & Winkler, 1991; Geiger, Stahl, & Rossman, 2000; Withers et al., 1998), pyrope-rich garnet (Mookherjee & Karato, 2010), natural grossular-rich garnet (e.g., Beran, Langer, & Andrut, 1993) and natural grossular (Rossman & Aines, 1991). Because the band at 3,570 ± 10 cm^{-1} was found in Ti-doped, synthetic pyrope (Geiger et al., 2000), it was regarded as a typical feature of garnet with ≥1 wt% TiO_2 (e.g., Geiger et al., 2000; Schmädicke et al., 2015). However, recent studies revealed that this band is also present in Ti-poor peridotitic garnet from CG (Padrón-Navarta & Hermann, 2017) and in eclogitic garnet with <0.1 wt% TiO_2 (Gose & Schmädicke, 2018). Accordingly, the latter authors argued that the band is possibly also caused by the hydrogarnet substitution, because its position is ver close to the wavenumber range of the 'hydrogarnet band' (i.e. 3,585–3,630 cm^{-1}) and the latter is known for changing its position along with garnet composition (e.g. Geiger et al., 1991; Rossman & Aines, 1991). If true, all bands in the 3,570–3,630 cm^{-1} range (summarized here as SW type II) may be related to the same type of substitution.

Recently, it was suggested (Geiger & Rossman, 2020) that all absorption bands due to structural OH in Dora Maira garnet (i.e. including the band at 3,650 cm^{-1}) could be related to the hydrogarnet substitution. In contrast, experiments on hydrogen diffusion in garnet of different composition, including Dora Maira specimens, imply different substitution mechanisms (e.g. Lu & Keppler, 1997; Padrón-Navarta, Hermann, & O'Neill, 2014; Reynes, Jollands, Hermann, & Ireland,

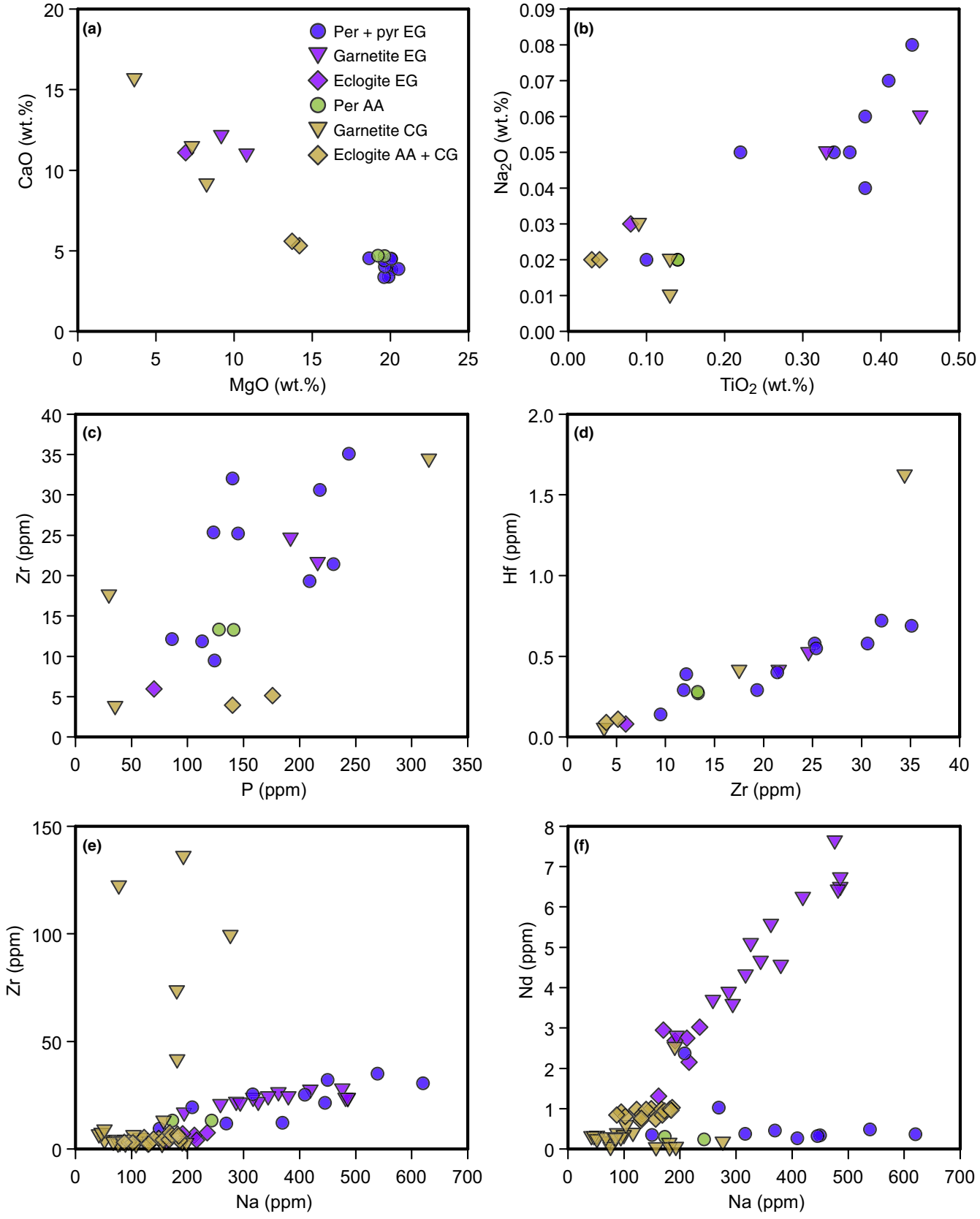

FIGURE 5 Binary scatter diagrams showing the average composition of garnet of peridotite-hosted garnetite and eclogite. (a) and (b) Sample averages of microprobe analyses; (c) to (f) trace element concentrations determined by ICP-MS. (c) and (d) are sample averages; (e) and (f) show results of individual spot analysis. Analyses of garnet in peridotite and pyroxenite (sample averages) are from Schmädicke and Gose (2019). AA, Alpe Arami; CG, Cima di Gagnone; EG, Erzgebirge; per, peridotite; pyr, pyroxenite; *r*, correlation coefficient

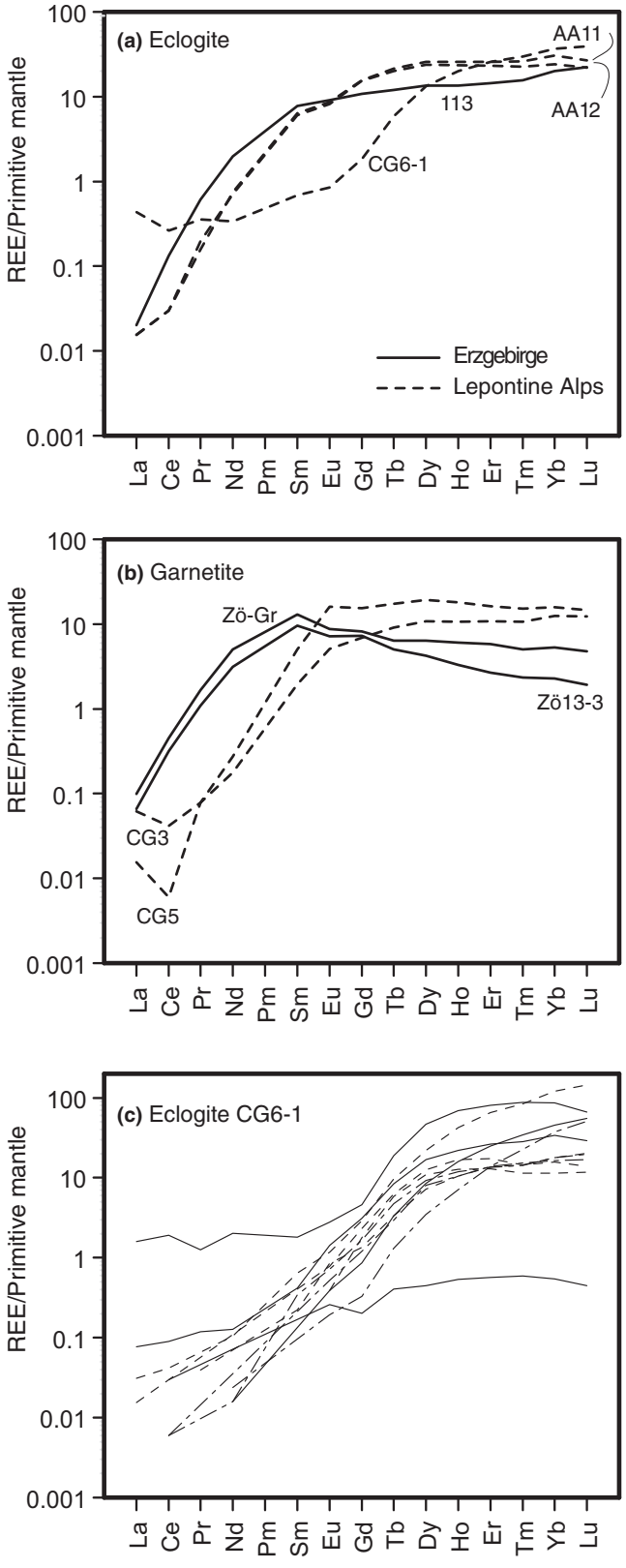

FIGURE 6 Normalized REE patterns for garnet using sample averages (a and b) or individual spot analyses (c). Normalization to primitive mantle (McDonough & Sun, 1995)

2018). The latter is supported by the observation that the SW I and SW II bands in our samples are differently influenced by secondary water (see Section 6.1).

5.3 | Water content and relation between water species

The water content in garnet inferred from both SW bands (I and II) is considerably higher in garnet from Erzgebirge samples than in those from the LA. Considering all analysed domains, the sample averages range from 124 to 258 ppm for EG samples and from 8 to 68 ppm for LA samples (Table 4). The H_2O concentration of a single sample is highly variable in EG samples (113:49–426 ppm; Zö13-3:76–222 ppm; Zö-Gr: 129–496 ppm) as well as in eclogite AA11 (0–195 ppm) from the LA. Notably, the variability in SW within a sample, commonly encompassing one order of magnitude, is much greater than the difference of average contents between samples. Importantly, those samples with large scatter of SW also have highly variable contents of molecular water. The latter points to inhomogeneously distributed sub-microscopic fluid inclusions with liquid water. Such inclusions are abundant in all EG samples and in eclogite AA11. In these samples, a single garnet grain may host domains being free of molecular water occurring next to grain portions with a few hundreds ppm of molecular water.

The above findings imply that part of the SW, especially in domains rich in molecular water, is most probably secondary (see Section 6.1). If only garnet domains with little or no molecular water (e.g. MW $\leq$ 20 ppm; Table 4) are considered, both the total content and the within-sample range of H_2O are significantly reduced in the inclusion-rich samples (i.e. samples 113, Zö13-3; Zö-Gr and AA11). Excluding all domains with MW > 20 ppm, the total amount of SW is still higher in Erzgebirge samples than in those from the LA. Comparing rock types, garnet from garnetite hosts more SW than eclogitic garnet. This applies to both the EG (garnetite: 121 and 241 ppm; eclogite: 84 ppm) and the LA samples (garnetite: 46 and 23 ppm; eclogite: 4, 8 and 11 ppm).

Moreover, the two SW bands show a marked contrast in intensity. Judging from the sample averages in Table 4, the much stronger SW II band accounts for 87%–96% of structural H_2O in the EG samples, no matter if MW-rich or -poor domains are considered. For LA samples, the contribution of SW II is somewhat smaller (i.e. 64%–87%). Furthermore, the scatter of the total SW contents in an individual garnet grain is mainly due to band SW II because it shows enormous intensity variation and the contribution of this band to the overall content of structural H_2O is much greater compared to band SW I (Table 4; Figures 8 and 9).

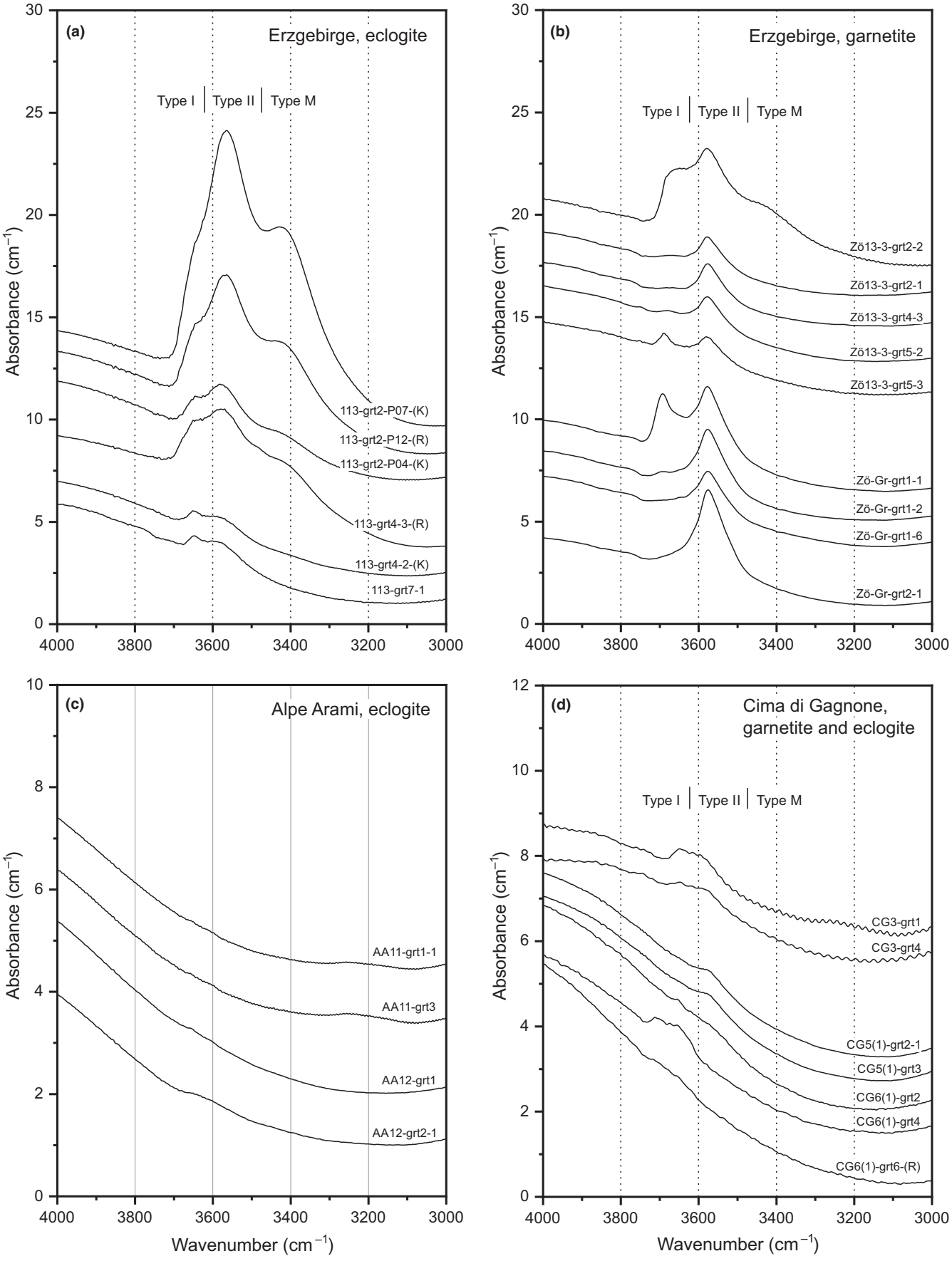

FIGURE 7 IR spectra of garnet from peridotite-hosted eclogite and garnetite (metarodingite) from the Erzgebirge (a, b) and the Lepontine Alps (c, d) normalized to 1 cm sample thickness

5.4 | Relation between SW and garnet composition

Using the average major and trace element composition of garnet in each sample, the content of primary SW is related to the mineral's composition, particularly its con

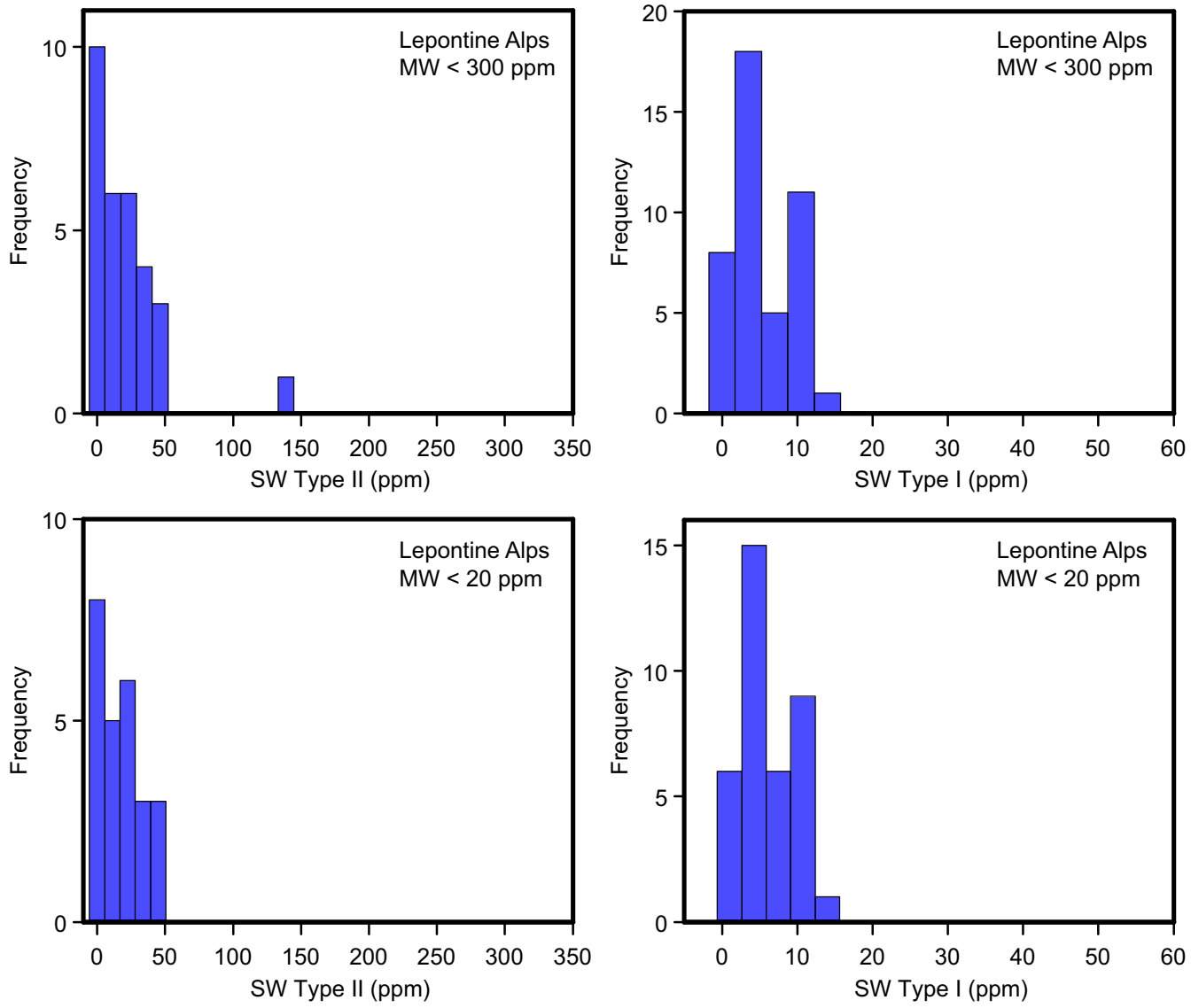

FIGURE 9 Histograms showing the concentration range and frequency of the two types of structural water, SW I and SW II, in garnet from peridotite-hosted eclogite and garnetite (metarodingite) from the Lepontine Alps. In contrast to the Erzgebirge, most samples contain very low amounts of molecular water (i.e. MW < 20 ppm); only very few have higher contents. This is the reason why the difference between the histograms for MW < 20 ppm and <300 ppm is much smaller than in Erzgebirge samples (Figure 8). As a consequence, the amount of secondary structural H_2O is negligible

6 | DISCUSSION AND CONCLUSIONS

6.1 | Primary SW

A pronounced relationship between structural and molecular water, as observed in this study, was previously reported for garnet from different rock types: Erzgebirge eclogite (e.g. Gose & Schmädicke, 2018), Erzgebirge and AA peridotite and pyroxenite (Schmädicke & Gose, 2019) as well as pyroxenite and eclogite xenoliths from the cratonic mantle (Schmädicke et al., 2015). In all former studies, the authors concluded that structural H_2O in garnet was secondarily

FIGURE 10 Sample average of primary structural H_2O (deduced from domains with <20 ppm MW) plotted against sample averages of CaO (a), Na_2O (b), TiO_2 (c), V (d), Th (e), Y (f), Ho (g) and Nd (h). The plots include the data of peridotite-hosted eclogite and garnetite (metarodingite) investigated in this study and the data for peridotite and pyroxenite (Schmädicke & Gose, 2019). AA, Alpe Arami; CG, Cima di Gagnone; EG, Erzgebirge; ecl, eclogite; gar, garnetite; per, peridotite; pyr, pyroxenite; *r*, orrelation coefficient. The dashed lines (a) visualize the trends for each the EG and the LA samples

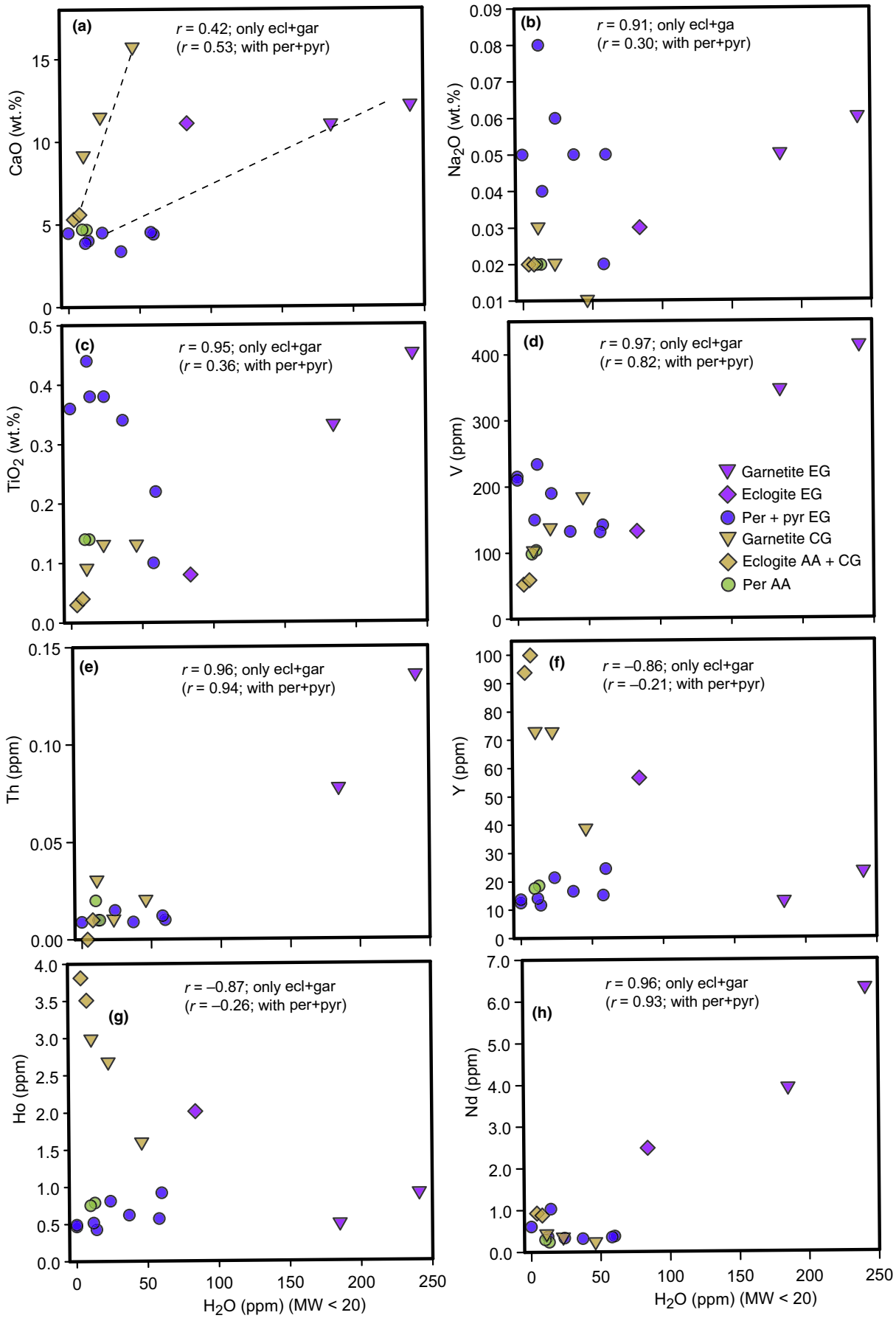
(a)
r = 0.42; only ecl+gar
(r = 0.53; with per+pyr)
CaO (wt.%)
(b)
r = 0.91; only ecl+ga
(r = 0.30; with per+pyr)
Na2O (wt.%)
(c)
r = 0.95; only ecl+gar
(r = 0.36; with per+pyr)
TiO2 (wt.%)
(d)
r = 0.97; only ecl+gar
(r = 0.82; with per+pyr)
V (ppm)
Garnetite EG
Eclogite EG
Per + pyr EG
Garnetite CG
Eclogite AA + CG
Per AA
(e)
r = 0.96; only ecl+gar
(r = 0.94; with per+pyr)
Th (ppm)
(f)
r = –0.86; only ecl+gar
(r = –0.21; with per+pyr)
Y (ppm)
(g)
r = –0.87; only ecl+gar
(r = –0.26; with per+pyr)
Ho (ppm)
(h)
r = 0.96; only ecl+gar
(r = 0.93; with per+pyr)
Nd (ppm)
H2O (ppm) (MW < 20)
H2O (ppm) (MW < 20)

enhanced by late-stage influx of water that was trapped in fluid inclusions. Accordingly, they inferred that the primary content of structural H_2O, corresponding either to peak-metamorphic (in case of orogenic rocks) or mantle conditions (in case of xenoliths) is only preserved in domains with little or no molecular water.

Because the present observations point in exactly the same direction (see Section 5.2), only garnet domains without molecular water or negligible amounts of it (MW ≤ 20 ppm; Table 4) are considered to reflect the primary amount of SW. The high contents of structural H_2O (up to c. 500 ppm; Table 4) in MW-rich domains (up to several hundred ppm MW) are ascribed to late-stage (relative to peak metamorphism) incorporation of secondary SW as a result of fluid influx. Moreover, this secondary SW is primarily incorporated in garnet by the substitution reflected by band SW II because the latter band is not only much stronger than the SW I band, but it is also much more variable in intensity (Figure 8).

Considering garnet domains with up to 300 ppm MW, the H_2O contents due to band SW II cover a large range from ~30 ppm to 330 ppm in the EG samples (Figure 8). The H_2O content from band SW I spans a narrower range from 0 to c. 56 ppm but, in most domains, it is <20 ppm. Considering only inclusion-poor domains (MW ≤ 20 ppm), the H_2O content due to the SW I band is not much different (~<17 ppm in most samples) compared to inclusion-rich domains. In contrast, the H_2O content due to band SW II is significantly reduced in inclusion-poor domains (i.e. 60–100 ppm in most cases). For samples from the LA, there is only little difference between domains with ≤20 ppm and up to 300 ppm molecular water, simply because MW-rich domains are very rare (Figure 9).

Having concluded that, in many garnet domains, part of the structural H_2O is secondary, especially in the Erzgebirge samples, the question remains why the two SW bands behave differently in relation to molecular water. Comparison with experimental data helps to tackle this subject and to disclose a possible linkage between water incorporation and physical conditions. In fact, HP experiments on natural, impure pyrope have shown that the SW bands at 3,650 cm^{-1} (our type I) and 3,600–3,630 cm^{-1} (our type II) differently respond to pressure (Lu & Keppler, 1997). While the total H_2O solubility in garnet positively correlates with pressure, only the intensity of band SW I increases with pressure, whereas that of band SW II decreases (Lu & Keppler, 1997). Accordingly, the authors inferred that the H_2O incorporation mechanism, generating band SW II (i.e. the hydrogarnet substitution; e.g. Geiger et al., 1991), is not favoured by high pressure, which they ascribed to the substitution-induced lattice increase.

Studies on natural garnet (Gose & Schmädicke, 2018; Schmädicke & Gose, 2017, 2019) and the present results point in the same direction, documenting that unusually high contents of SW in garnet are invariably associated with an intense SW II band. In addition, the latter is particularly strong in domains rich in molecular water. Hence, we conclude that part of the SW bound by the hydrogarnet substitution was incorporated during decompression as a result of the influx of H_2O-rich fluid. The latter was trapped as fluid inclusions in garnet, which, in turn, enhanced the incorporation of secondary SW in the vicinity of such inclusions resulting in enormous grain-scale variations of structural H_2O. As a consequence, the primary amount of intrinsic water related to peak metamorphism can only be deduced from garnet domains without fluid inclusions. It is, however, possible that even some of such inclusion-free domains may be influenced by secondary SW, namely in the case that fluid inclusions occur in the vicinity (but not within) of the probed crystal volume.

6.2 | Water loss and degree of H_2O undersaturation

The possibility that garnet could have lost some of its primary water due to decompression was recently evaluated for garnet from ultramafic rocks that are derived from the same two field areas as the samples from this study (Schmädicke & Gose, 2019). Based on several arguments, which are also applicable to the present samples, the authors concluded that water loss is very unlikely. Apart from the fact that hydrogen diffusion can be as slow as that of other cations, depending on the OH substitution type and oxygen fugacity (e.g. Padrón-Navarta et al., 2014; Reynes et al., 2018), pyropic garnet shows little difference in the H_2O storage capacity in the pressure interval between 30 and 15 kbar (Lu & Keppler, 1997). As a result, diffusional water loss should not occur during decompression from UHP conditions to, at least, 15 kbar. At lower pressure and simultaneously reduced temperature, hydrogen diffusion and water loss should be kinetically restricted. The most important reason, however, is that water loss due to pressure release cannot be reconciled with a renewed uptake of secondary SW during decompression. In principle, water loss is only possible in the case that the H_2O content in garnet is equal to or higher than its H_2O storage capacity, that is, the maximum amount that a mineral is able to incorporate in its structure at given PT conditions. If this capacity decreases due to decompression, SW is released from an originally saturated mineral. However, no water loss will occur from a mineral that is undersaturated with respect to its storage capacity. For the present samples, the uptake of secondary water signifies that garnet cannot have been H_2O-saturated, with the implication that decompressional water loss can be excluded in the present case.

Experimental data would be helpful to evaluate the degree of water undersaturation. Unfortunately, such data are sparse and the garnet samples used in experimental studies are compositionally very different from our samples. Garnet from Dora Maira (Lu & Keppler, 1997) may give some clues in this context even though the CaO content of the latter (0.6 wt%) is at least one order of magnitude lower compared to our samples (5–17 wt%). The study found that H_2O in garnet increases with pressure and does not depend on temperature (at least in the studied range between 800 and 1,200°C). At 30 kbar, Dora Maira pyrope was found to host 50–60 ppm H_2O at saturated conditions. Considerably more water should be storable in garnet as Ca-rich as our samples (e.g. Rossman & Aines, 1991). The fact that part of our samples contain even less than 50–60 ppm water independently signals severe H_2O deficiency.

Further evidence for H_2O-undersaturated conditions is provided by literature data on garnet peridotite from CG (Padrón-Navarta & Hermann, 2017). Peridotitic garnet contains 6 ppm H_2O, which is only 10% of the amount expected for Ca-poor, pyropic garnet that equilibrated at 15–30 kbar. The low water content of coexisting orthopyroxene (i.e. 13 ppm) supports this conclusion because several studies have shown that the mineral is able to incorporate about 300 ppm in spinel peridotite and even more H_2O at pressure conditions of the garnet-peridotite facies (e.g. Demouchy, Shcheka, Denis, & Thoraval, 2017; Rauch & Keppler, 2002; Schmädicke, Gose, & Stalder, 2018; Stalder, Karimova, & Konzett, 2015). Olivine, on the other hand, hosts 20 or 31 ppm H_2O (depending on calibration), which is unusually high. This high amount may be due to the high Ti content or could be related to uptake of secondary SW, facilitated by the much higher diffusivity of hydrogen in olivine relative to orthopyroxene and garnet (e.g. Blanchard & Ingrin, 2004; Demouchy & Mackwell, 2006; Peslier & Luhr, 2006; Schmädicke, Gose, Witt-Eickschen, & Brätz, 2013; Stalder & Skogby, 2003).

6.3 | Implications of REE patterns

Garnet with MREE humps or sinusoidal-shaped REE patterns, occur in the garnetite, but not the eclogite samples from the Erzgebirge and the LA (Figure 6). Such features are relatively common in eclogite xenoliths from the cratonic mantle (Bell et al., 2005; Bizimis, Salters, & Bonatti, 2000; Schmädicke et al., 2015; Simon, Carlson, Pearson, & Davies, 2007; Stachel et al., 2004). The MREE humps are ascribed to metasomatic enrichment of MREE by a hydrous fluid or melt by most authors; sinusoidal patterns, on the other hand, may be caused by either metasomatic enrichment of LREE or depletion of MREE. Although the present samples testify to the infiltration of hydrous fluid, as documented by garnet-hosted inclusions of molecular water, the observed anomalous REE patterns in garnet from garnetite cannot be related to this stage of fluid influx. This is because such fluid inclusions are absent in many garnet grains that are characterized by an anomalous REE distribution. Vice versa, numerous fluid inclusions occur in eclogitic garnet, but the REE curves of the latter (Figure 6) are 'normal' and parallel to those of garnet from the host peridotite (Schmädicke & Gose, 2019) both bearing no sign of metasomatic enrichment or depletion of REE.

In conclusion, the observations imply that the metasomatic enrichment process that led to the anomalous REE distribution cannot be related to the incorporation of molecular water as inclusions in garnet. The consequence of this reasoning is that the rocks must have been influenced by at least two independent, fluid-driven processes that occurred at different stages during the evolution of the rocks. As inferred above, the incorporation of molecular water in garnet resulted from the influx of hydrous fluid at post-peak metamorphic conditions. In contrast, fluid-mediated metasomatism that affected the REE patterns must have occurred prior to peak metamorphism. Due to the fact that eclogite was not affected, metasomatism, most probably, took place on the ocean floor and was related to rodingitization of the basaltic or gabbroic protoliths of garnetite.

6.4 | Garnet composition and water content

Comparison of the present results with recently published data on water in natural garnet from HP rocks of the same field areas, including peridotite, pyroxenite and gneiss-hosted eclogite from Erzgebirge and peridotite from AA (Gose & Schmädicke, 2018; Schmädicke & Gose, 2017, 2019), helps to evaluate if garnet composition controls the incorporation of SW. Because those literature data are from rocks belonging to the same units and having shared their metamorphic history with the present samples, possible differences in the water content of garnet cannot be attributed to differences in *P* and/or *T* but should be related to its composition.

The literature data reveal that, in eclogitic and peridotitic garnet, H_2O correlates with Ca, Na, Ti, V, P, Zr, Y and REE. However, the present results imply that such correlation trends cannot be a unique feature of (U)HP garnet but seem to depend on the rock type. In the present sample set, for instance, a clear positive correlation of H_2O is found for Na, Ti and V but not for both P and Zr. Instead, correlative trends of B, Ga, Pb, Th and U with H_2O are observed that have not been described yet for garnet from other locations (as far as the authors are aware). Moreover, some elements like Ti, V, Y and HREE are positively correlated with H_2O in one sample set and negatively in another. For example, the present data for garnet in garnetite and eclogite reveal a positive trend for Ti and V and a negative one for Y and HREE; in contrast

peridotitic and pyroxenitic garnet from the same occurrences (Schmädicke & Gose, 2019) shows the opposite: positive correlation for Y and HREE and a negative one for Ti and V.

In conclusion, the contrasting relation of H_2O with respect to several trace elements (such as Ti, V, P, Zr, Y and REE) in garnet of different sample sets is a strong indication that H_2O is not a function of these elemental concentrations. Instead, the relation between garnet composition and water content seems to be governed by an independent parameter related to petrogenesis. It has been argued that water in garnet from gneiss-hosted eclogite primarily stems from an internal source (see below). In fact, the contrasting correlation trends seem to support this suggestion. Supposing that water is internally produced from decomposing hydrous minerals, the reaction pathway and the composition of the dehydrating mineral(s) are the key parameters that determine which trace elements are liberated and available to be incorporated in the remaining minerals along with water.

Furthermore, a positive correlation between H_2O and CaO, as documented for garnet from gneiss-hosted EG eclogite (Gose & Schmädicke, 2018), is not observed here if all samples are combined (Figure 10a). However, if the EG and LA samples are separated, a positive H_2O-CaO correlation becomes obvious for each of the field areas (Figure 10a). Based on this result, again, the question arises if the H_2O content in garnet is solely governed by crystal chemistry. In fact, the observed disparity between the EG and LA samples regarding the CaO-H_2O correlation suggests, at least, that crystal chemistry cannot be the only influential parameter. In addition, the above mentioned contrasting correlation trends for minor and trace elements point in the same direction, casting doubts on a simple dependence of structural H_2O in garnet on the mineral's composition. Thus, other variables, specifically the availability of water during peak metamorphism, have to be taken into account (Gose & Schmädicke, 2018).

As demonstrated in a study on EG eclogite, the H_2O content in garnet as well as its correlation with CaO, is governed by the PT evolution and the resulting metamorphic reaction history (Gose & Schmädicke, 2018). In fact, the availability of water at peak metamorphic conditions is a function of both (a) the reaction pathway, controlling dehydration reactions and the internal liberation of H_2O and (b) the stability or instability of hydrous minerals in the peak metamorphic assemblage, which, in turn, is governed by peak pressure (Gose & Schmädicke, 2018; Schmädicke & Gose, 2017). This explains why garnet in common coesite eclogite, in which hydrous minerals were not stable during peak metamorphism, contains much more water (50–180 ppm) than garnet in quartz eclogite (8–28 ppm; Gose & Schmädicke, 2018) that equilibrated with calcic amphibole, zoisite and minor phengite (Gose & Schmädicke, 2018). Apart from controlling the co-stability of hydrous minerals, however, peak pressure seems to play only a minor (if any) role for water incorporation in garnet, because the H_2O content in garnet from quartz eclogite samples with different peak pressure is indistinguishable (Gose & Schmädicke, 2018). In addition, garnet of an exceptional coesite eclogite with peak-metamorphic phlogopite is equally H_2O-poor as garnet of quartz eclogite.

In accordance with these findings, we conclude that the higher H_2O content in garnet from the Erzgebirge rocks (garnetite: 121 and 241 ppm; eclogite 84 ppm) compared to equivalents from the LA (garnetite: 23 and 46 ppm; eclogite: 4, 8 and 11 ppm) may be a result of the observed instability (EG samples) or stability (LA samples) of hydrous minerals such as calcic amphibole, zoisite (in eclogite and garnetite) and phengite (in eclogite) in the peak metamorphic assemblage.

6.5 | Petrogenetic implications

This study reveals differences in the H_2O content of garnet between the Erzgebirge (more H_2O) and the LA (less H_2O) as well as between eclogite (less H_2O) and garnetite (more H_2O). Notably, also samples with relatively high contents of primary SW are H_2O-deficient. The finding that garnet from garnetite hosts more SW than eclogitic garnet applies to both the EG and the LA samples and is attributed to the mineral's higher CaO content. The positive correlation between H_2O and CaO, including not only garnet from eclogite and garnetite but also from peridotite (Figure 10a; see above), signifies that all three associated types of rocks are characterized by roughly the same degree of H_2O-undersaturation. Again, this points to a shared metamorphic evolution of eclogite, garnetite (metarodingite) and peridotite. In addition, the presence of two separate H_2O-CaO correlation trends for EG and LA samples suggests that the water content in natural garnet cannot be solely governed by its Ca concentration. Although the latter may determine the H_2O storage capacity, the actual water content of garnet seems to be strongly dependent on the availability of water at peak metamorphic conditions. Notably, the samples from both the Erzgebirge and the LA testify to water deficiency during peak metamorphism, albeit to different degrees of undersaturation, which we ascribe to the lack (EG) or the co-stability (LA) of hydrous minerals in the peak assemblage.

The novel result that garnet in both eclogite and garnetite from the Erzgebirge and the LA incorporated less SW at peak metamorphism compared to the H_2O storage capacity at these conditions, has important genetic implications. Notably, the H_2O deficiency applies to garnet from all mafic and ultramafic rock types, as indicated by the uptake of secondary SW during decompression. The latter is impossible for an H_2O-saturated mineral, which would be subject to decompressional water loss, not gain. In addition, garnet in peridotite-hosted EG eclogite (84 ppm) is as water-poor as that in gneiss-hosted eclogite occurring in the same UHP unit (50–180 ppm; Gose & Schmädicke, 2018).

These findings, together with the ubiquitous water-deficiency in all studied Erzgebirge rocks, including peridotite (Schmädicke & Gose, 2019), eclogite and garnetite, is not compatible with the derivation of these rocks from the mantle wedge. This is because a subducting slab incorporates only material from the lowermost portion of the overlying mantle, which is expected to be rich in water, if not watersaturated. Instead, we suggest that gneiss-hosted coesite eclogite as well as peridotite-hosted eclogite, garnetite and the host peridotite itself, which are all part of the Erzgebirge UHP unit, not only followed the same metamorphic evolution (Schmädicke et al., 1992; Schmädicke & Evans, 1997) but also shared a common origin, most probably on the ocean floor. This inference is in line with the mere presence of garnetite, which was interpreted as metarodingite (Schmädicke & Evans, 1997) supporting a low-pressure, ocean-floor origin of the protoliths similarly as proposed for equivalent rocks from CG, LA (Evans & Trommsdorff, 1978; Evans et al., 1979). For the same reasons, it is also possible that the protoliths of eclogite and peridotite from AA shared a low-pressure, ocean-floor origin. However, because metarodingite is not known from Alpe Arami, in contrast to the Erzgebirge and Cima di Gagnone, this hypothesis needs to be tested by further investigations.

ACKNOWLEDGEMENTS

We thank two anonymous reviewers for their fair, constructive reviews as well as Donna L. Whitney for editorial handling. We are also indebted to Helene Brätz (Erlangen) for help with the ICP analyses and to Roland Stalder (Innsbruck) for providing the analytical facilities for the IR measurements. Funding by Deutsche Forschungsgemeinschaft (grant Schm1039/9-1) is gratefully acknowledged.

ORCID

Esther Schmädicke https://orcid.org/0000-0002-0522-8210

REFERENCES

Becker, H. (1993). Garnet peridotite and eclogite Sm-Nd mineral ages from the Lepontine dome (Swiss Alps): New evidence for Eocene high-pressure metamorphism in the central Alps. *Geology*, *21*(7), 599–602. https://doi.org/10.1130/0091-7613(1993)021<0599:GPAESN>2.3.CO;2

Bell, D. R., Grégoire, M., Grove, T. L., Chatterjee, N., Carlson, R. W., & Buseck, P. R. (2005). Silica and volatile-element metasomatism of Archean mantle: A xenolith-scale example from the Kaapvaal Craton. *Contributions to Mineralogy and Petrology*, *150*, 251–267. https://doi.org/10.1007/s00410-005-0673-8

Bell, D. R., Ihinger, P. D., & Rossman, G. R. (1995). Quantitative analysis of trace OH in garnet and pyroxenes. *American Mineralogist*, *80*, 465–474. https://doi.org/10.2138/am-1995-5-607

Beran, A., Langer, K., & Andrut, M. (1993). Single crystal infrared spectra in the range of OH fundamentals of paragenetic garnet, omphacite and kyanite in an eklogitic mantle xenolith. *Mineralogy and Petrology*, *48*, 257–268. https://doi.org/10.1007/BF01163102

Bizimis, M., Salters, V. J. M., & Bonatti, E. (2000). Trace and REE content of clinopyroxene from supra-subduction zone peridotites. Implications for melting and enrichment processes in island arcs. *Chemical Geology*, *165*, 67–85.

Blanchard, M., & Ingrin, J. (2004). Hydrogen diffusion in Dora Maira pyrope. *Physics and Chemistry of Minerals*, *31*, 593–605. https://doi.org/10.1007/s00269-004-0421-z

Brenker, F. E., & Brey, G. P. (1997). Reconstruction of the exhumation path of the Alpe Arami garnet peridotite body from depths exceeding 160 km. *Journal of Metamorphic Geology*, *15*, 581–592. https://doi.org/10.1111/j.1525-1314.1997.tb00637.x

Brenker, F. E., Müller, W. F., & Brey, G. P. (2003). Variation of antiphase domain size in omphacite: A tool to determine the temperature–time history of eclogites revisited. *American Mineralogist*, *88*, 1300–1311. https://doi.org/10.2138/am-2003-8-912

Brueckner, H. K. (1998). Sinking intrusion model for the emplacement of garnet-bearing peridotites into continent collision orogens. *Geology*, *26*, 631–634. https://doi.org/10.1130/0091-7613(1998)026<0631:SIMFTE>2.3.CO;2

Brueckner, H. K., Carswell, D. A., Griffin, W. L., Medaris, L. G., Van Roermund, H., & Cuthbert, S. J. (2010). The mantle and crustal evolution of two garnet peridotite suites from the Western Gneiss Region, Norwegian Caledonides: An isotopic investigation. *Lithos*, *117*, 1–19. https://doi.org/10.1016/j.lithos.2010.01.011

Coleman, R. G. (1971). Plate tectonic emplacement of upper mantle peridotites along continental edges. *Journal of Geophysical Research*, *6*, 1212–1222.

Demouchy, S., & Mackwell, S. (2006). Mechanisms of hydrogen incorporation and diffusion in iron-bearing olivine. *Physics and Chemistry of Minerals*, *33*, 347–355. https://doi.org/10.1007/s00269-006-0081-2

Demouchy, S., Shcheka, S., Denis, C. M. M., & Thoraval, C. (2017). Subsolidus hydrogen partitioning between nominally anhydrous minerals in garnet-bearing peridotite. *American Mineralogist*, *102*, 1822–1183. https://doi.org/10.2138/am-2017-6089

Evans, B. W., & Trommsdorff, V. (1978). Petrogenesis of garnet lherzolite, Cima di Gagnone, Lepontine Alps. *Earth and Planetary Science Letters*, *40*, 333–348. https://doi.org/10.1016/0012-821X(78)90158-9

Evans, B. W., Trommsdorff, V., & Richter, W. (1979). Petrology of an eclogite-metarodingite suite at Cima di Gagnone, Ticino, Switzerland. *American Mineralogist*, *64*, 15–31.

Geiger, C. A., Langer, K., Bell, D. R., Rossman, G. R., & Winkler, B. (1991). The hydroxide component in synthetic pyrope. *American Mineralogist*, *76*, 49–59.

Geiger, C. A., & Rossman, G. R. (2020). Micro- and nano-size hydrogarnet clusters and proton ordering in calcium silicate garnet: Part I. The quest to understand the nature of "water" in garnet continues. *American Mineralogist*, *105*(4), 455–467.

Geiger, C. A., Stahl, A., & Rossman, G. R. (2000). Single-crystal IR and UV/VIS-spectroscopic measurements on transition-metal-bearing pyrope: The incorporation of hydroxide in garnet. *European Journal of Mineralogy*, *12*, 259–271. https://doi.org/10.1127/0935-1221/2000/0012-0259

Gose, J., & Schmädicke, E. (2018). Water incorporation in garnet: Coesite versus Quartz eclogite from Erzgebirge and Fichtelgebirge. *Journal of Petrology*, *59*, 207–232. https://doi.org/10.1093/petrology/egy022

Green, H. W., Dobrzhintskaya, L. F., & Bozhilov, K. N. (2010). The Alpe Arami story: Triumph of data over prejudice. *Journal of Earth Science*, *21*, 731–743. https://doi.org/10.1007/s12583-010-0130-0

Heinrich, C. A. (1982). Kyanite-eclogite to amphibolite fades evolution of hydrous mafic and pelitic rocks, Adula Nappe, Central Alps. *Contributions to Mineralogy and Petrology*, *81*, 30–38. https://doi.org/10.1007/BF00371156

Heinrich, C. A. (1986). Eclogite facies regional metamorphism of hydrous mafic rocks in the Central Alpine Adula nappe. *Journal of Petrology*, *27*, 123–154. https://doi.org/10.1093/petrology/27.1.123

Hermann, J., O'Neill, H. S. C., & Berry, A. J. (2005). Titanium solubility in olivine in the system TiO_2-MgO-SiO_2: No evidence for an ultra-deep origin of Ti-bearing olivine. *Contributions to Mineralogy and Petrology*, *148*, 746–760. https://doi.org/10.1007/s00410-004-0637-4

Herwartz, D., Nagel, T. J., Münker, C., Scherer, E. E., & Froitzheim, N. (2011). Tracing two orogenic cycles in one eclogite sample by Lu–Hf garnet chronometry. *Nature Geoscience*, *4*, 178–183. https://doi.org/10.1038/ngeo1060

Klemd, R., & Schmädicke, E. (1994). High-pressure metamorphism in the Münchberg Gneiss Complex and the Erzgebirge Crystalline Complex: The roles of fluid and reaction kinetics. *Geochemistry – Chemie Der Erde*, *54*, 241–261.

Lu, R., & Keppler, H. (1997). Water solubility in pyrope to 100 kbar. *Contributions to Mineralogy and Petrology*, *129*, 35–42. https://doi.org/10.1007/s004100050321

Massonne, H.-J. (2001). First find of coesite in the ultrahigh-pressure metamorphic region of the Central Erzgebirge, Germany. *European Journal of Mineralogy*, *13*, 565–570.

Mathé, G. (1990). Zur Geologie der Serpentinitvorkommen im sächsischen Erzgebirge. *Abhandlungen Des Staatlichen Museums Für Mineralogie Und Geologie Dresden*, *37*, 55–72.

McDonough, W. F., & Sun, S. S. (1995). The composition of the Earth. *Chemical Geology*, *120*, 223–253. https://doi.org/10.1016/0009-2541(94)00140-4

Medaris, L. G., Wang, H. F., Misar, Z., & Jelinek, E. (1990). Thermobarometry, diffusion modelling and cooling rates of crustal garnet peridotites: Two examples from the Moldanubian zone of the Bohemian Massif. *Lithos*, *25*, 189–201. https://doi.org/10.1016/0024-4937(90)90014-R

Möckel, J. R. (1969). Structural petrology of the garnet-peridotite of Alpe Arami (Ticino, Switzerland). *Leidse Geologische Mededelingen*, *42*, 61–130.

Mookherjee, M., & Karato, S. (2010). Solubility of water in pyrope-rich garnet at high pressures and temperatures. *Geophysical Research Letters*, *37*(L03310). https://doi.org/10.1029/2009GL041289

Nasdala, L., & Massonne, H.-J. (2000). Microdiamonds from the Saxonian Erzgebirge, Germany: In situ micro-Raman characterization. *European Journal of Mineralogy*, *12*, 495–498.

Nimis, P., & Trommsdorff, V. (2001). Revised thermobarometry of Alpe Arami and other garnet peridotites from the Central Alps. *Journal of Petrology*, *42*, 103–115. https://doi.org/10.1093/petrology/42.1.103

O'Hara, M. J., & Mercy, E. L. (1966). Garnet peridotite and eclogite from Bellinzona, Switzerland. *Earth and Planetary Science Letters*, *1*, 61–130. https://doi.org/10.1016/0012-821X(66)90011-2

Padrón-Navarta, A. J., Hermann, J., & O'Neill, H. S. O. (2014). Site-specific hydrogen diffusion rates in forsterite. *Earth and Planetary Science Letters*, *392*, 100–112. https://doi.org/10.1016/j.epsl.2014.01.055

Padrón-Navarta, J. A., & Hermann, J. (2017). A Subsolidus olivine water solubility equation for the Earth's upper mantle. *Journal of Geophysical Research*, *122*(12), 9862–9880. https://doi.org/10.1002/2017JB014510

Paquin, J., & Altherr, R. (2001). New constraints on the P-T evolution of the Alpe Arami garnet peridotite body (Central Alps, Switzerland). *Journal of Petrology*, *42*, 1119–1140. https://doi.org/10.1093/petrology/42.6.1119

Peslier, A. H. (2010). A review of water contents of nominally anhydrous natural minerals in the mantles of Earth, Mars and the Moon. *Journal of Volcanology and Geothermal Research*, *197*, 239–258. https://doi.org/10.1016/j.jvolgeores.2009.10.006

Peslier, A., & Luhr, J. F. (2006). Hydrogen loss from olivine in mantle xenoliths from Simcoe (USA) and Mexico: Mafic alkalic magma ascent rates and water budget of the sub-continental lithosphere. *Earth and Planetary Science Letters*, *242*, 302–319.

Pfiffner, M., & Trommsdorff, V. (1998). The high-pressure ultramafic-mafic-carbonate suite of Cima Lunga-Adula, Central Alps: Excursions to Cima di Gagnone and Alpe Arami. *Schweizerische Mineralogische Und Petrographische Mitteilungen*, *78*(2), 337–354.

Rauch, M., & Keppler, H. (2002). Water solubility in orthopyroxene. *Contributions to Mineralogy and Petrology*, *143*, 525–536. https://doi.org/10.1007/s00410-002-0365-6

Reynes, J., Jollands, M., Hermann, J., & Ireland, T. (2018). Experimental constraints on hydrogen diffusion in garnet. *Contributions to Mineralogy & Petrology*, *173*, 69.

Rossman, G. R., & Aines, R. D. (1991). The hydrous components in garnets: Grossular-hydrogrossular. *American Mineralogist*, *76*, 153–1164.

Sandmann, S., Nagel, T. J., Herwartz, D., Fonseca, R. O. C., Kurzawski, R. M., Münker, C., & Froitzheim, N. (2014). Lu–Hf garnet systematics of a polymetamorphic basement unit: New evidence for coherent exhumation of the Adula Nappe (Central Alps) from eclogite-facies conditions. *Contributions to Mineralogy and Petrology*, *168*, 1075. https://doi.org/10.1007/s00410-014-1075-6

Scambelluri, M., Hermann, J., Morten, L., & Rampone, E. (2006). Melt- versus fluid-indiced metasomatism in spinel to garnet wedge peridotites (Ulten Zone, Eastern Italien Alps): Clues from trace element and Li abundances. *Contributions to Mineralogy and Petrology*, *151*, 372–394.

Scambelluri, M., Pettke, T., Rampone, E., Godard, M., & Reusser, E. (2014). Petrology and trace element budgets of high-pressure peridotites indicate subduction dehydration of serpentinized mantle (Cima di Gagnone, Central Alps, Switzerland). *Journal of Petrology*, *55*, 459–498. https://doi.org/10.1093/petrology/egt068

Schmädicke, E. (1991). Quartz pseudomorphs after coesite in eclogites from the Saxonian Erzgebirge. *European Journal of Mineralogy*, *3*, 231–238. https://doi.org/10.1127/ejm/3/2/0231

Schmädicke, E. (1994). Die Eklogite des Erzgebirges. In TU Bergakademie Freiberg (Ed.), *Freiberger Forschungsheft C456* (338 pp). Leipzig-Stuttgart: Deutscher Verlag für Grundstoffindustrie

Schmädicke, E., & Evans, B. W. (1997). Garnet-bearing ultramafic rocks from the Erzgebirge, and their relation to other settings in the Bohemian Massif. *Contributions to Mineralogy and Petrology*, *127*, 57–74. https://doi.org/10.1007/s004100050265

Schmädicke, E., & Gose, J. (2017). Water transport by subduction: Clues from garnet of Erzgebirge UHP eclogite. *American Mineralogist*, *102*, 975–986. https://doi.org/10.2138/am-2017-5920

Schmädicke, E., & Gose, J. (2019). Low water contents in garnet of orogenic peridotite: Clues for an abyssal or mantle-wedge origin?

European Journal of Mineralogy, *31*(4), 715–730. https://doi.org/10.1127/ejm/2019/0031-2880

Schmädicke, E., Gose, J., Reinhardt, J., Will, T. M., & Stalder, R. (2015). Garnet in cratonic and non-cratonic mantle and lower crustal xenoliths from southern Africa: Composition, water incorporation and geodynamic constraints. *Precambrian Research*, *270*, 285–299. https://doi.org/10.1016/j.precamres.2015.09.019

Schmädicke, E., Gose, J., & Stalder, R. (2018). Water in abyssal peridotite: Why are melt-depleted rocks so water rich? *Geochemistry, Geophysics, Geosystems*, *19*, 1824–1843. https://doi.org/10.1029/2017GC007390.

Schmädicke, E., Gose, J., & Will, T. M. (2010). The P-T evolution of ultra high temperature garnet-bearing ultramafic rocks from the Saxonian Granulitgebirge Core Complex, Bohemian Massif. *Journal of Metamorphic Geology*, *28*, 489–508. https://doi.org/10.1111/j.1525-1314.2010.00876.x

Schmädicke, E., Gose, J., Witt-Eickschen, G., & Brätz, H. (2013). Olivine from spinel peridotite xenoliths: Hydroxyl incorporation and mineral composition. *American Mineralogist*, *98*, 1870–1880. https://doi.org/10.2138/am.2013.4440

Schmädicke, E., Mezger, K., Cosca, M. A., & Okrusch, M. (1995). Variscan Sm-Nd and Ar-Ar ages of eclogite-facies rocks from the Erzgebirge, Bohemian Massif. *Journal of Metamorphic Geology*, *13*, 537–552. https://doi.org/10.1111/j.1525-1314.1995.tb00241.x

Schmädicke, E., Okrusch, M., & Schmidt, W. (1992). Eclogite-facies rocks in the Saxonian Erzgebirge, Germany: High pressure metamorphism under contrasting P-T conditions. *Contributions to Mineralogy and Petrology*, *110*, 226–241. https://doi.org/10.1007/BF00310740

Schmädicke, E., Will, T. M., Ling, X., Li, X.-H., & Li, Q. (2018). Rare peak and ubiquitous post-peak zircon in eclogite: Constraints for the timing of UHP and HP metamorphism in Erzgebirge, Germany. *Lithos*, *322*, 250–267. https://doi.org/10.1016/j.lithos.2018.10.017

Schmid, S. M., Pfiffner, O. A., Froitzheim, N., Schönborn, G., & Kissling, E. (1996). Geophysical-geological transect and tectonic evolution of the Swiss-Italian Alps. *Tectonics*, *15*, 1036–1064. https://doi.org/10.1029/96TC00433

Simon, N. S. C., Carlson, R. W., Pearson, D. G., & Davies, G. R. (2007). The origin and evolution of the Kaapvaal cratonic lithospheric mantle. *Journal of Petrology*, *48*, 589–625. https://doi.org/10.1093/petrology/egl074

Skogby, H., Bell, D. R., & Rossman, G. R. (1990). Hydroxide in pyroxene: Variations in the natural environment. *American Mineralogist*, *75*, 764–774.

Stachel, T., Aulbach, S., Brey, G. P., Harris, J. W., Leost, I., Tappert, R., & Viljoen, K. S. (2004). The trace element composition of silicate inclusions in diamonds: A review. *Lithos*, *77*, 1–19. https://doi.org/10.1016/j.lithos.2004.03.027

Stalder, R., Karimova, A., & Konzett, J. (2015). OH-defects in multiple-doped orthoenstatite at 4–8 GPa: Filling the gap between pure and natural systems. *Contributions to Mineralogy and Petrology*, *169*, 38.

Stalder, R., & Skogby, H. (2003). Hydrogen diffusion in natural and synthetic orthopyroxene. *Physics and Chemistry of Minerals*, *30*, 12–19. https://doi.org/10.1007/s00269-002-0285-z

Stöckhert, B., Duyster, J., Trepmann, C., & Massonne, H. J. (2001). Microdiamond daughter crystals precipitated from supercritical COH silicate fluids included in garnet, Erzgebirge, Germany. *Geology*, *29*, 391–394. https://doi.org/10.1130/0091-7613(2001)029<0391:MDCPFS>2.0.CO;2

Trommsdorff, V. (1990). Metamorphism and tectonics in the Central Alps: The Alpine lithospheric mélange of Cima Lunga and Adula. *Memorie Della Societá Geologica Italiana*, *45*, 39–49.

Trommsdorff, V., Hermann, J., Münterer, O., Pfiffner, M., & Risold, A. C. (2000). Geodynamic cycles of subcontinental lithosphere in the Central Alps and the Arami enigma. *Journal of Geodynamics*, *30*, 77–92. https://doi.org/10.1016/S0264-3707(99)00028-9

Van Achterbergh, E., Ryan, C. G., & Griffin, W. L. (2000). GLITTER: On-Line Interactive Data Reduction for the Laser Ablation ICP-MS Microprobe. In 9th Annual V.M. Goldschmidt Conference 25, 305–306. Macquarie University.

Whitney, D. L., & Evans, B. W. (2010). Abbreviations for names of rock-forming minerals. *American Mineralogist*, *95*, 185–187. https://doi.org/10.2138/am.2010.3371

Withers, A. C., Wood, B. J., & Carroll, M. R. (1998). The OH content of pyrope at high pressure. *Chemical Geology*, *147*, 161–171. https://doi.org/10.1016/S0009-2541(97)00179-4

Yu, M., Wang, Q., & Yang, J. (2019). Fabrics and water contents of peridotites in the Neotethyan Luobusa ophiolite, southern Tibet: Implications for mantle recycling in supra-subduction zones. *Journal of the Geological Society*, *176*, 975–991. https://doi.org/10.1144/jgs2018-152

How to cite this article: Schmädicke E, Gose J. Water in garnet of garnetite (metarodingite) and eclogite from the Erzgebirge and the Lepontine Alps. *J Metamorph Geol*. 2020;38:905–933. https://doi.org/10.1111/jmg.12554